

19 **ABSTRACT**

20

21 The Fossil Bluff Group of eastern Alexander Island records the exceptional preservation of more
22 than 8 km of Mesozoic sedimentary rocks deposited into an accretionary forearc basin that
23 developed unconformably above a late Paleozoic accretionary complex, and in proximity to a
24 continental margin arc during a prolonged phase of enhanced magmatism. Through the Mesozoic,
25 the Fossil Bluff Group evolved from a trench-slope environment to a forearc basin sourced from the
26 continental margin arc. During this period, the Antarctic Peninsula's convergent margin was
27 characterized by episodes of magmatic flare-ups that developed during tectonic compression,
28 crustal thickening, extension, and uplift. U-Pb and Lu-Hf detrital zircon data are used to determine
29 the provenance of the forearc succession and as a monitor for arc magmatic tempos during the late
30 Mesozoic. The magmatic record in the adjacent arc is poorly preserved or partially absent, but the
31 sedimentary record of the forearc basin preserves a largely uninterrupted record of arc magmatism
32 that can be studied with detrital zircon geochronology and geochemistry. The basal succession of the
33 Fossil Bluff Group is sourced from the adjacent accretionary complex, but thereafter it is strongly
34 controlled by the proximal arc in western Palmer Land and is characterised by a mixed arc/recycled
35 signature during episodes of renewed sedimentation. However the main phases of deposition during
36 the Early Jurassic (ca. 180 Ma), Early Cretaceous (141 – 131 Ma), and mid-Cretaceous (125 – 102 Ma)
37 are dominated by arc-only sources. The Lu-Hf isotopic record supports a transition from convergence
38 to extension and a return to convergence during the Mesozoic, which is consistent with accretionary
39 orogens from elsewhere along the West Gondwanan margin. The provenance record during the
40 depositional history of the basin points overwhelmingly to an autochthonous origin; as such, models
41 for parts of the western province of the Antarctic Peninsula being allochthonous are unsupported.

42

43 1. INTRODUCTION

44 The Mesozoic Fossil Bluff Group of the Antarctic Peninsula preserves the accumulation of >8 km
45 of arc-derived material into a forearc basin that developed unconformably above a late Paleozoic –
46 Mesozoic accretionary complex (LeMay Group). The Fossil Bluff Group is exposed along the eastern
47 margin of Alexander Island (Figs. 1, 2, 3) in a narrow belt, ~250 km-long belt. The forearc succession
48 of Alexander Island is interpreted to continue north (Fig. 1) into Adelaide Island (Riley et al., 2012)
49 and the South Shetland Islands (Bastias et al., 2023) and potentially forms components of the
50 Magallanes-Austral Basin (Dobbs et al., 2022), although the geology is mostly obscured. The
51 succession has a depositional history from the Early Jurassic to the mid-Cretaceous and forms one of
52 the most complete ancient forearc successions in the world (Doubleday et al., 1993). However,
53 despite many authors having investigated the lithostratigraphy (e.g. Butterworth et al., 1988), fossil
54 record (e.g. Crame and Howlett, 1988), and tectonic development (e.g. Storey et al., 1996), the
55 origin of the basin and its provenance remains uncertain. Addressing these aspects is central to
56 understanding the tectonic and magmatic history of the West Gondwanan margin, its subsequent
57 break-up and the formation of the Antarctic Peninsula.

58 Vaughan and Storey (2000) interpreted Alexander Island as a possible exotic terrane (Western
59 Domain; Fig. 1) that accreted to the Antarctic Peninsula during the Early to mid-Cretaceous. This was
60 a period of global plate reorganization (Matthews et al., 2012) and coincided with an Early to mid-
61 Cretaceous magmatic “flare-up” event in the Antarctic Peninsula (Riley et al. 2018) that can be
62 traced from Patagonia (Pankhurst et al., 1999) through West Antarctica (Siddoway et al., 2005) and
63 New Zealand (Milan et al., 2017). Vaughan et al., (2012) identified a pronounced mid-Cretaceous
64 compressional event that led to deformation and terrane translation along the West Gondwanan
65 margin (Vaughan and Storey, 2000; Vaughan et al., 2002; Guenther et al., 2010; Riley et al., 2023).
66 Commenting on the deformational history of the Fossil Bluff Group, Nell and Storey (1991)
67 suggested that strike-slip motion along the LeMay Range Fault, which separates the LeMay Group

68 accretionary complex from the Fossil Bluff Group forearc succession (Fig. 2), had a long history. The
69 LeMay Range Fault initially formed as a dextral strike-slip fault owing to the oblique subduction of
70 the Phoenix Plate. These conditions are conducive to the translation of forearc slivers and terrane
71 displacement (Jarrard, 1986). Therefore, a key question is whether the Fossil Bluff Group succession
72 was deposited *in situ*. Recent contributions have tended to favour an *in situ* continental arc setting
73 (Burton-Johnson and Riley, 2015; Gao et al., 2021; Bastias et al., 2021), although Riley et al. (2023)
74 suggested a para-autochthonous origin for at least parts of the western margin of the Antarctic
75 Peninsula, with accretion developing after 90 Ma.

76 To explain more about the origin of the Fossil Bluff Group and the contemporaneous magmatic
77 history of the adjacent arc, this study examined the detrital zircon U-Pb record of the forearc
78 succession from basal units overlying the LeMay Group accretionary complex to the uppermost
79 sequences along the eastern margin of Alexander Island. Using U-Pb zircon age profiles and Lu-Hf
80 isotopes we investigated the source of material into the forearc basin and evaluated the likely
81 depositional age of the succession and basin formation. Evaluating the complete record of the
82 forearc basin through the late Mesozoic allows a more detailed understanding of the magmatic
83 evolution of the continental margin arc and episodes of uplift and erosion. The new detrital zircon
84 geochronological data allowed us to produce an updated geological map of the entire Fossil Bluff
85 Group and refine the boundaries between different formations (Fig. 3).

86

87 **2. GEOLOGICAL SETTING**

88 **2.1 Antarctic Peninsula**

89 The Antarctic Peninsula has a geological history that extends back to the Ordovician (Fig. 1) and is
90 marked by a series of magmatic, tectonic, and depositional events that developed in an accretionary
91 continental margin setting in West Gondwana (Smellie, 2021). Vaughan et al. (2002) suggested that
92 the Antarctic Peninsula developed through a process of terrane translation and accretion onto the

93 West Gondwanan margin, although more recent contributions favour an autochthonous continental
94 arc setting (e.g. Bastias et al., 2021).

95

96 **2.2. Alexander Island**

97 The geology of Alexander Island (Fig. 2) can be divided into four geological units: (1) a late
98 Paleozoic – early Mesozoic accretionary complex (LeMay Group; Riley et al., 2023) in
99 unconformable/faulted contact with (2) a shallowing forearc basin/trench slope sedimentary
100 succession at least 8 km in thickness (Fossil Bluff Group; this study). The LeMay Group is intruded by
101 (3) Late Cretaceous – Cenozoic granites, and locally overlain by volcanic units of the same age
102 (McCarron and Millar, 1997). (4) The final geological unit on Alexander Island is an episode of
103 Neogene – Quaternary (7 – 0.1 Ma) alkaline volcanism that erupted following the end of subduction;
104 it forms two separate volcanic fields in northern and southwestern Alexander Island (Fig. 2) that are
105 part of the Bellingshausen Sea volcanic field (Smellie and Hole, 2021).

106 Vaughan and Storey (2000) interpreted Alexander Island as either a subduction-accretionary
107 complex to the para-autochthonous/allochthonous Central Domain (Fig. 1) or as an allochthonous
108 exotic terrane (Western Domain; Fig. 1) that “docked” with the Antarctic Peninsula during the mid-
109 Cretaceous Palmer Land Event (Vaughan et al., 2012). Collision with the Antarctic Peninsula may
110 have occurred farther south than its current position, with continental margin parallel translation
111 taking place along a large-scale dextral shear zone (Vaughan and Storey, 2000). There are several
112 advantages to a segmented model for the Antarctic Peninsula and an allochthonous Central-Western
113 Domain. Subduction geometry and granitoid chemistry for Antarctic Peninsula Mesozoic magmatism
114 is more straightforward to explain with a trench closer to Palmer Land, as opposed to a greater
115 lateral distance when the Central-Western Domain occupies its current position (Bastias et al.,
116 2023). Also, a terrane translation model for the Antarctic Peninsula is consistent with mid-
117 Cretaceous tectonic models elsewhere along the West Gondwanan margin (e.g. New Zealand;
118 Robertson et al., 2019). However, an allochthonous model for the Central-Western Domain with a

119 mid-Cretaceous suturing is difficult to reconcile with certain aspects of geochronology and
120 aeromagnetic data across putative terrane boundaries (Burton-Johnson and Riley, 2015). In this
121 paper, we will examine the juxtaposition between Alexander Island and the Antarctic Peninsula and
122 the relationship between the LeMay Group and Fossil Bluff Group and arc magmatism of Palmer
123 Land, and whether a suspect terrane model is appropriate for the Western Domain.

124 The deformational history of the forearc succession has been investigated by Doubleday and
125 Storey (1998) who examined successions from the Middle Jurassic to the mid-Cretaceous. They
126 identified three distinct deformational events: (1) Middle Jurassic strike-slip movement on the
127 LeMay Range Fault (Fig. 2) in the accretionary complex; (2) forearc basin inversion in the mid-
128 Cretaceous that developed in a dextral transpressional setting; and (3) post-inversion extension,
129 which was the final deformational phase, and postdates the depositional history of the Fossil Bluff
130 Group; this phase led to the opening of the George VI Sound rift (Fig. 2). Doubleday and Storey
131 (1998) attributed phase 1 to be related to oblique subduction, whilst basin inversion (phase 2) was a
132 Pacific-wide, mid-Cretaceous compressional event. This is consistent with calculated convergence
133 rates in Riley et al. (2020a) and Burton-Johnson et al. (2022), which demonstrated an increase in
134 convergence post-140 Ma. The later transtensional phase of deformation was interpreted by Nell
135 and Storey (1991) to be related to oblique subduction after 50 Ma, or potentially due to ridge
136 segment-trench collision that resulted in the cessation of subduction at ca. 30 Ma (Larter and Barker,
137 1991). However, Jordan et al. (2014) determined that arc magmatism on Adelaide Island continued
138 until at least ca. 23 Ma. This later event was highlighted by Twinn et al. (2022), who identified an
139 episode of accelerated cooling at ca. 25 Ma (apatite thermochronometry) that was associated with
140 trench collision of a spreading ridge segment.

141

142 **2.3 Fossil Bluff Group and Sample Information**

143 The forearc basin clastic sedimentary succession of the Fossil Bluff Group unconformably overlies,
144 and is in faulted contact with, the accretionary LeMay Group (unit 1 in Fig. 3). There are several

145 localities west of Planet Heights (Fig. 3) where rocks of the Fossil Bluff Group rest unconformably on
146 the LeMay Group (Edwards, 1979; Tranter, 1987). At the boundary between the two groups it is
147 evident that the LeMay Group was deformed prior to deposition of the Fossil Bluff Group (Storey
148 and Nell, 1988), whilst elsewhere the boundary is a major fault (LeMay Range Fault; Edwards, 1979).

149 The Fossil Bluff Group was initially defined by Butterworth et al. (1988), but has been revised
150 several times and is now defined as an ~8 km succession of clastic units that record a transition from
151 trench slope to forearc basin deposition as part of a major shallowing sequence. At least 11
152 separate, mappable units have been identified across the Fossil Bluff Group (Fig. 3), with deposition
153 likely to extend from the Bajocian (ca. 170 Ma) to the Albian (ca. 100 Ma) based on biostratigraphy
154 and lithostratigraphy (e.g. Doubleday et al., 1993; Crame and Francis, 2024), although the main
155 phase of forearc deposition probably developed through the mid-Cretaceous. The forearc succession
156 is best defined as a compressional accretionary basin with landward migration of the depo-center
157 (cf. Noda, 2016) and episodes of extension. The geological map of the Fossil Bluff Group is shown in
158 Figure 3 with the depositional age primarily constrained by molluscan fossils and plant material
159 (Butterworth et al., 1988), but it was adapted following the analysis presented here.

160 Samples for detrital zircon (U-Pb and Lu-Hf) analysis were selected from across the Fossil Bluff
161 Group (Fig. 2) to examine their provenance through the entire depositional history of the succession.
162 Fifteen samples were selected for analysis from eastern Alexander Island, with samples from the
163 lowermost Selene Nunatak Formation and uppermost Neptune Glacier Formation included (Fig. 3).
164 Several samples were also examined from the basin-wide Himalia Ridge Formation. A detailed and
165 revised geological map and sample locations are shown in Fig. 3. Precise positional information is
166 provided for all samples in the Supplemental Material.

167 The lowermost succession of the Fossil Bluff Group is the Selene Nunatak Formation (unit 2 in Fig.
168 3), which forms a narrow north-south-trending unit in the central part of the succession (Fig. 3). The
169 sequence is ~150 m in thickness, with the type section defined from Selene Nunatak (Fig. 3) where

170 the unit unconformably overlies the accretionary complex of the LeMay Group (unit 1 in Fig. 3). The
171 Selene Nunatak Formation is characterised by pebble-cobble conglomerate (sedimentary clasts),
172 that is associated with laminated mudstones and coarser units (Doubleday et al., 1993). Two
173 samples for detrital zircon analysis were selected from the Selene Nunatak Formation from the
174 western end of Nonplus Crag, north of the type locality at Selene Nunatak (Fig. 3). Samples
175 **KG.4640.33** and **KG.4640.44** are medium- to coarse-grained sandstones, which have a weakly
176 developed structural fabric.

177 The Atoll Nunataks Formation (unit 3 in Fig. 3) conformably overlies the Selene Nunatak
178 Formation and forms a sequence ~1000 m in thickness, with its type section exposed to the east of
179 Atoll Nunataks (Fig. 3). Holdsworth and Nell (1992) interpreted the Atoll Nunataks Formation as a
180 trench-slope sequence that dips beneath parts of the forearc basin and may pre-date the formation
181 of the “true” forearc succession. The Atoll Nunataks Formation dips moderately to the east and has
182 no penetrative fabric, although the sequence is characterised by irregular fractures and joints.
183 Sample **KG.3669.24** near Lunar Crag (Fig. 3) is from a coarse-grained sandstone interbed with small
184 sedimentary pebble clasts.

185 The Ablation Point Formation (unit 4 in Fig. 3) is confined to the eastern margin of Alexander
186 Island between Jupiter Glacier and Belemnite Point (Taylor et al., 1979), with the type section
187 defined from Ablation Point (Fig. 3). At Ablation Point, the sequence has a minimum thickness of 350
188 m, but reaches a thickness of 440 m at the nearby Himalia Ridge (Fig. 3). The Ablation Point
189 Formation comprises a zone of highly disturbed and brecciated sediments, which have been
190 interpreted as a syn-sedimentary *mélange* (Macdonald and Butterworth, 1986). Sample **KG.3657.4** is
191 a medium-grained sandstone from a sandstone-mudstone interbed adjacent to a minor thrust fault.
192 The unit is host to poorly preserved perisphinctid ammonites. The extent of the Ablation Point
193 Formation is also interpreted to continue across King George VI Sound into northwest Palmer Land
194 (Taylor et al., 1979) at Carse Point, where sandstone sample **R.2151.30** is located (Fig. 2).

195 The Himalia Ridge Formation (unit 5 in Fig. 3) is the only unit of the Fossil Bluff Group that is
196 basin-wide, with the type section defined from Himalia Ridge (Fig. 3), where a maximum thickness of
197 ~2600 m has been recorded, although elsewhere, the Himalia Ridge Formation has a thickness in the
198 range of 1000 – 1500 m (Butterworth et al., 1988).

199 The Himalia Ridge Formation has a variable stratigraphy and is characterised by a broad range of
200 different facies with considerable lateral variation. The unit consists of four major conglomerate
201 beds that form prominent steep scarps. The conglomerate beds are 80 – 170 m in thickness (Miller
202 and Macdonald, 2004) and are channeled with westward paleoflow indicators that suggest a source
203 direction from the magmatic arc to the east. At its type section, three distinct pulses of coarse-
204 grained sediment input have been recognised, which are interpreted to reflect tectonic allocyclic
205 control and to be related to uplift in the hinterland (Butterworth, 1991). Significant arc uplift is also
206 supported by a shift in conglomerate clast composition from volcanic to plutonic. This is also
207 reflected in the sandstone petrofacies that trend from undissected arc to dissected arc/basement
208 uplift, which Butterworth (1991) attributed to arc unroofing.

209 Macdonald et al. (1999) identified ocean island basalt-like rocks that were contemporaneous with
210 the deposition of the Himalia Ridge Formation and were used as evidence of a dynamic rift-setting
211 for forearc basin development.

212 In the upper part of the Himalia Ridge Formation, the Jupiter Glacier Member (unit 5a in Fig. 3)
213 crops out at Callisto Cliffs and consists of fine-grained laminated sandstones that represent an
214 abrupt, but temporary, regional shallowing event.

215 Three samples were analysed from the Himalia Ridge Formation and were collected from the
216 Ganymede Heights-Ablation Valley area (Fig. 3). Samples **KG.2883.4** and **KG.3069.2** from Ablation
217 Valley are medium- to coarse-grained sandstones that crop out above a minor thrust zone. Sample
218 **KG.3463.3** is a collection of several granitoid cobbles from a conglomerate bed at Ganymede
219 Heights.

220 The Spartan Glacier Formation (unit 6 in Fig. 3) is approximately 1 km in thickness and its type
221 locality crops out to the south of Spartan Glacier (Butterworth et al., 1988). The formation is
222 characterised by mudstone and siltstone with minor, fine-grained sandstone interbeds. The Spartan
223 Glacier Formation is host to a broad molluscan fauna, but is not particularly age diagnostic, although
224 an Early Cretaceous (Berriasian–Hauterivian) age is suggested (Crame and Howlett, 1988).

225 There is a clear transition from the uppermost Himalia Ridge Formation/Jupiter Glacier Member
226 to the Spartan Glacier Formation in terms of sediment supply, which shifts from clastic gravels to
227 fine-grained lithologies. Butterworth (1991) determined that the Spartan Glacier Formation was
228 deposited in a tectonically quiescent setting, although slope-collapse deposits and local angular
229 unconformities indicate some tectonic control.

230 Two samples were analysed from the Spartan Glacier Formation (unit 6). Sample **KG.3231.2**, from
231 Leda Ridge (Fig. 3), near Ganymede Heights, is a medium-grained graded sandstone, while
232 **KG.3968.2** is from a narrow band of the Spartan Glacier Formation near Offset Ridge (Fig. 3) and is a
233 siltstone/fine-grained sandstone.

234 The Pluto Glacier Formation (unit 7 in Fig. 3) is exposed extensively across the southern sector of
235 the Fossil Bluff Group and has a total thickness of up to 2500 m (Moncrieff and Kelly, 1993). The
236 succession is characterised by a high proportion of fine- to medium-grained sandstones that are
237 locally cross-bedded and bioturbated (Moncrieff and Kelly, 1993). The Pluto Glacier Formation is an
238 extensive shelf sandstone/deltaic unit that may have a diachronous relationship with deltaic and
239 terrestrial sequences farther south (Butterworth, 1991).

240 The Rhea Corner Member (unit 7a) is a distinct unit in the Pluto Glacier Formation and occurs in
241 the upper part of the succession at Rhea Corner (Fig. 3). It forms a 370 m thick sandy and
242 conglomeratic unit, with a strongly erosive base and contrasts with the dominantly finer grained
243 lithology of the Pluto Glacier Formation.

244 Three samples were analysed from the Pluto Glacier Formation (unit 7). Sample **KG.3969.1**, near
245 Astarte Horn (Fig. 3), is adjacent to the contact with the LeMay Group accretionary complex. The
246 sample is a cross-bedded coarse siltstone from a reverse faulted slice of the Pluto Glacier Formation
247 in faulted contact with the LeMay Group. Sample **KG.3959.2** is a medium-grained sandstone bed
248 from the Pluto Glacier Formation at Offset Ridge (Fig. 3), whilst **KG.4109.1** is a medium-grained and
249 well-bedded sandstone from Pickering Nunataks (Fig. 3).

250 The uppermost 2500 m of the Fossil Bluff Group forms the Neptune Glacier Formation, which has
251 been split into three separate units (Fig. 3). The Deimos Ridge Member (unit 8 in Fig. 3) crops out
252 south of the Venus Glacier and forms a 700-m-thick succession of predominantly sandstone with
253 mudstone interbeds. The Milestone Bluff Formation of central Adelaide Island, ~120 km north of
254 Alexander Island (Fig. 1), forms a succession at least 1500 m in thickness of sandy, turbiditic
255 sedimentary units with minor interbedded crystal and vitric tuff units and has been correlated to the
256 Deimos Ridge Member (Riley et al., 2012). Cobble and boulder conglomerates form prominent units
257 of up to 20 m in thickness, and clast orientations suggest a source to the east. Riley et al. (2012)
258 dated a crystal tuff bed from the Milestone Bluff Formation at 113.9 ± 1.2 Ma.

259 One sample was examined here to investigate the potential correlation of the Alexander Island
260 and Adelaide Island sectors of the forearc basin. Sample **J6.288.2** is a matrix-supported pebble
261 conglomerate (dominantly volcanic clasts) from Milestone Bluff (Fig. 1).

262 The Triton Point Member (unit 9; Fig. 3) has a total thickness of ~800 m and crops out at Triton
263 Point and farther south at Coal and Titan nunataks where the unit is thickest (Nichols and Cantrill,
264 2002). It is characterised by standing trees at the base of the succession and marine fauna from near
265 the top which support a late Albian age (Crame and Howlett, 1988). Sample **KG.4956.1** is a coarse-
266 grained sandstone bed from the upper part of a ~700 m thick succession at Coal Nunatak.

267 There is an abrupt change in facies from the Deimos Ridge Member to the Triton Point Member,
268 with an erosion surface marking the base of a braided fluvial channel sandstone unit. Uplift prior to

269 the incised river channels led to subaerial conditions and plant roots are evident (Nichols and
270 Cantrill, 2002). Paleocurrent evidence from Moncrieff and Kelly (1993) and Nichols and Cantrill
271 (2002) demonstrates sediment input from the arc to the east, but transport to the southwest in the
272 south and to the northwest in the north, which developed across a braided plain delta extending
273 approximately 30 km to the north and west.

274 The uppermost unit of the Fossil Bluff Group is the Mars Glacier Member (unit 10 in Fig. 3), which
275 crops out from Triton Point to Two Step Cliffs (Fig. 3). This unit forms a sequence of up to 1000 m in
276 thickness and is dominated by medium-grained sandstones with subordinate mudstones and
277 conglomerates and is characterised by fossil forest horizons (Nichols and Cantrill, 2002). No samples
278 were examined from the Mars Glacier Member as part of this study.

279

280 **3. ANALYTICAL METHODS**

281 **3.1 U-Pb Zircon Geochronology**

282 Zircon (U-Pb) geochronology was conducted at the Swedish Museum of Natural History and
283 University College London. Full analytical procedures, data (Table S2) and cathodoluminescence
284 images (Fig. S1) from each laboratory are provided in the Supplementary Material, but a summary of
285 the analytical procedures is provided here.

286 At the Swedish Museum of Natural History (Stockholm), U-Pb ion-microprobe zircon
287 geochronology was carried out using a CAMECA 1280 ion microprobe at the NordSIMS facility. The
288 analytical method closely followed Whitehouse and Kamber (2005) but differs inasmuch that the
289 oxygen ion primary beam was generated using a high-brightness, radiofrequency (RF) plasma ion
290 source (Oregon Physics, Hyperion II, rather than a duoplasmatron) and a focused beam instead of an
291 illuminated aperture. The 10 nA O₂-beam was rastered over 5x5 µm to homogenize beam density,
292 and the final analytical spot size was ~15 µm in diameter. Sputtered secondary ions introduced into
293 the mass spectrometer were analyzed using a single ion-counting electron multiplier over 10 cycles

294 of data. Data were reduced using software developed in-house. The power law relationship between
295 $^{206}\text{Pb}/^{238}\text{U}^{16}\text{O}$ and $^{238}\text{U}^{16}\text{O}_2/^{238}\text{U}^{16}\text{O}$ measured from the 91500 standard was used to calibrate U/Pb
296 ratios following the recommendations of Jeon and Whitehouse (2015). Common-Pb corrections
297 were applied to analyses where statistically significant ^{204}Pb was detected, using the present-day
298 terrestrial common Pb estimate of Stacey and Kramers (1975). ^{207}Pb corrected ages were calculated
299 assuming non-radiogenic Pb was from surface contamination and had an isotopic composition of
300 modern-day average terrestrial common-Pb ($^{207}\text{Pb}/^{206}\text{Pb} = 0.836$; Stacey and Kramers, 1975).

301 Zircon U–Pb geochronology at University College London was conducted using laser ablation
302 inductively coupled plasma–mass spectrometry (LA-ICP-MS; an Agilent 7700 coupled to a New Wave
303 Research 193 nm excimer laser) at the London Geochronology Center. Typical laser spot sizes of 25
304 μm were used with a 7–10 Hz repetition rate and a fluence of 2.5 J/cm². Background measurement
305 before ablation lasted 15 s and the laser ablation dwell time was 25 s. The external zircon standard
306 was Plešovice, which has a thermal ionization mass spectrometry (TIMS) reference age of $337.13 \pm$
307 0.37 Ma (Sláma et al., 2008). Standard errors on isotopic ratios and ages include the standard
308 deviation of $^{206}\text{Pb}/^{238}\text{U}$ ages of the Plešovice standard zircon. Time-resolved signals that record
309 isotopic ratios with depth in each crystal were processed using GLITTER 4.5, data reduction software,
310 developed by the ARC National Key Center for Geochemical Evolution and Metallogeny of Continents
311 (GEMOC) at Macquarie University and the Commonwealth Scientific and Industrial Research
312 Organisation (Australia) Exploration and Mining division. Processing enabled filtering to remove
313 spurious signals resulting from overgrowth boundaries, weathering, inclusions, and fractures. Ages
314 were calculated using the $^{206}\text{Pb}/^{238}\text{U}$ ratios for samples younger than 1.1 Ga, and the $^{207}\text{Pb}/^{206}\text{Pb}$
315 ratios for older grains. Discordance was determined using $((^{207}\text{Pb}/^{235}\text{U} - ^{206}\text{Pb}/^{238}\text{U}) / ^{206}\text{Pb}/^{238}\text{U})$ and
316 for $^{207}\text{Pb}/^{206}\text{Pb}$ ages.

317

318 **3.2 Lu-Hf Isotopic Analysis**

319 Lu-Hf isotopes were determined on a subset of those samples analysed for their U-Pb age, and
320 analysis was conducted using the same spot as was used for U-Pb geochronology. Eight samples
321 were selected for analysis to provide a good representation through the Fossil Bluff Group
322 succession. The analyses were determined on a Neptune multicollector–inductively coupled plasma
323 – mass spectrometer (ICP-MS) coupled with a laser ablation system at the British Geological Survey,
324 Keyworth, UK. Initial $^{176}\text{Hf}/^{177}\text{Hf}$ ratios were calculated using the U-Pb crystallisation age of each
325 grain, and the results are expressed as initial ϵHf (ϵHf_i). ϵHf values were calculated using a ^{176}Lu
326 decay constant of $1.867 \times 10^{-11}\text{y}^{-1}$ (Söderlund et al., 2004), the present-day chondritic $^{176}\text{Lu}/^{177}\text{Hf}$
327 value of 0.0336, and an $^{176}\text{Hf}/^{177}\text{Hf}$ ratio of 0.282785 (Bouvier et al., 2008). Full analytical details are
328 provided in the supplementary files and the data are provided in the Supplemental Material Table,
329 and the data are presented in Table S3.

330

331 **4. RESULTS**

332 **4.1 U-Pb Detrital Zircon Geochronology**

333 The age distributions of all 15 samples analyzed are plotted in Figure 4 as probability density plots
334 (after Vermeesch, 2018), overlain with kernel density estimator curves. Overall, there is significant
335 variation across the Fossil Bluff Group, with a clear younging age distribution towards the eastern
336 part of the succession and certain units displaying a broader pattern of older zircon grains. Two
337 samples (KG.4640.33 and KG.4640.44) from the Selene Nunatak Formation (unit 2) from the base of
338 the Fossil Bluff Group have the broadest spread of detrital zircon ages (Figs. 4A and 4B) of all the
339 analysed samples, with a prominent Late Permian age peak at ca. 265 Ma and a significant range of
340 ages through the Palaeozoic. The age distribution, with a prominent Late Permian peak is akin to the
341 adjacent LeMay Group accretionary complex (Riley et al., 2023), although a younger age of
342 deposition for the Selene Nunatak Formation is indicated by rare zircon grains that record ages
343 younger than 220 Ma. The age distribution is characteristic of a strong local bias with a proximal

344 source to sink depositional environment. The detrital zircon population is broadly consistent with a
345 possible Bajocian bio-stratigraphical age for the Selene Nunatak Formation (ca. 170 Ma;
346 Butterworth, 1991).

347 The sample from unit 3 (Atoll Nunataks Formation) records a very different age profile than those
348 samples from the underlying Selene Nunatak Formation. Sample KG.3669.24 has a prominent Early
349 Jurassic age peak of ca. 183 Ma and a secondary Triassic age peak at ca. 204 Ma (Fig. 4C). No
350 Palaeozoic age populations are identified in sample KG.3669.24, which indicates that there is no
351 contribution from the proximal LeMay Group accretionary complex or the underlying Selene
352 Nunatak Formation. The age profile is consistent with a likely Bajocian – Bathonian depositional age
353 (ca. 177 Ma; Fig. S2), which places it in the lower part of the Atoll Nunataks Formation. The detrital
354 zircon age population presented here is not in agreement with the interpretation of Doubleday et al.
355 (1993), who interpreted that the Atoll Nunataks Formation was derived from the proximal LeMay
356 Group accretionary complex. The complete absence of Permian zircon grains in sample KG.3669.24
357 of the Atoll Nunataks Formation indicates no source relationship to the LeMay Group.

358 The Ablation Point Formation is restricted to eastern Alexander Island, and also the western
359 margin of northwest Palmer Land at Carse Point (Fig. 2). Two samples (KG.3657.4 and R.2151.30)
360 from the Ablation Point Formation share very similar age profiles in the interval 217–207 Ma,
361 characterized by prominent Late Jurassic (ca. 155 Ma) age peaks and well-defined Triassic peaks (Fig.
362 4D and 4E). Both samples yield maximum likely depositional ages of ca. 155 Ma (Fig. S2). The sample
363 from north of Belemnite Peak (KG.3657.4) has a broader age profile, with zircons from the
364 Carboniferous and Ordovician. A depositional age of ca. 155 Ma is also supported by its suspected
365 Kimmeridgian fauna (Crame and Howlett, 1988). The age profile from the sandstone at Carse Point
366 (sample R.2151.30) has a more localised depositional signature, with no significant regional
367 component that is characteristic of the adjacent sample near Belemnite Point (sample KG.3657.4).

368 The Himalia Ridge Formation (unit 5) is basin-wide, and two samples (KG.2883.4 and KG.3069.2)
369 from close to the type locality record very similar age profiles. Both samples have prominent Early
370 Cretaceous age peaks of ca. 143 Ma, with a secondary peak shoulder at ca. 138 Ma (Figs. 4F and 4G)
371 and yield maximum depositional ages of c. 140 Ma (Supplementary Figure 2). The Himalia Ridge
372 Formation is also characterised by a mid-Triassic signal at c. 213 Ma, akin to the Ablation Point
373 Formation and a peak at c. 182 Ma that is also evident in the Atoll Nunataks Formation. Granitoid
374 clasts from a conglomerate (sample KG.3463.2) from the Himalia Ridge Formation record a single
375 age peak at ca. 140 Ma (Fig. 4H), which indicates likely supply from a distinct erosional level and
376 correlates with the primary detrital zircon age peaks from the sandstone samples of the Himalia
377 Ridge Formation. The granitoid-dominant conglomerate unit is typical of the upper part of the
378 Himalia Ridge Formation, with its source from a deeper erosional level (Butterworth, 1991).

379 The Spartan Glacier Formation shares a distribution of ages similar to that of the underlying
380 Himalia Ridge Formation. Two samples from the Spartan Glacier Formation were analysed from
381 almost opposite ends of the lateral extent of the unit (Fig. 3). Sample KG.3968.2 is located at the
382 southern extent of the Spartan Glacier Formation, ~85 km south of sample site KG.3231.2. Despite
383 the distance between sample sites, both share very similar age distribution profiles, with prominent
384 Early Cretaceous age peaks (143 – 136 Ma; Figs. 4I and 4J) and a broader distribution of ages through
385 the Early Jurassic (ca. 184 Ma) and the mid-Triassic (ca. 218 Ma). Both samples have a broad
386 distribution of recycled zircon grains, which indicates a degree of exhumation and erosion of
387 basement material.

388 Three samples from the Pluto Glacier Formation exhibit very similar age distributions (Figs. 4K
389 and 4M). Two samples (KG.3959.2 and KG.4109.6) are from the main succession of the Pluto Glacier
390 Formation, whilst sample KG.3969.1 is from a reverse faulted slice farther west. All are characterised
391 by a prominent Early to mid-Cretaceous age peak at ca. 126 Ma that constitutes ~90% of the detrital
392 zircon population and likely indicates a depositional environment with a prominent local bias, but
393 with a minor component of recycled basement material. This yields likely maximum depositional

394 ages in the range of 129 – 124 Ma, which are broadly consistent with a Lower Aptian age (ca. 120
395 Ma) suggested by the molluscan fauna (Crame and Howlett, 1988), although a Barremian–Aptian age
396 maybe more appropriate given the older maximum depositional ages.

397 Two samples from the uppermost Neptune Glacier Formation were analysed, including one
398 sample from the forearc basin extension into Adelaide Island (J6.288.2 of the Milestone Bluff
399 Formation) and one from the Triton Peak Member at Coal Nunatak (Fig. 3; sample KG.4956.1). The
400 detrital zircon age profiles are consistent with the stratigraphy, with J6.288.2 displaying two
401 prominent Early to mid-Cretaceous age peaks at ca. 112 Ma and ca. 134 Ma (Fig. 4N), whilst sample
402 KG.4956.1 is characterised by a major peak at ca. 105 Ma and a secondary peak at ca. 124 Ma (Fig.
403 4O). The age profiles are consistent with a local bias and no significant regional contribution from
404 basement sources. These ages also correlate well with the biostratigraphy, which suggests
405 deposition during the Albian.

406

407 **4.2 Lu-Hf Isotopes**

408 Lu-Hf isotopic analysis was conducted out on a subset of the Fossil Bluff Group samples that was
409 analyzed for U-Pb geochronology. Eight samples were selected for analysis from the Fossil Bluff
410 Group to provide good representation across the succession. All zircon grains analysed for U-Pb
411 geochronology were selected for Lu-Hf analysis (Supplementary Table 3).

412 The lowermost succession analysed was the Atoll Nunataks Formation (sample KG.3669.24),
413 which yields ϵ_{Hf} values in the range of -6 to 0 for the Early Jurassic age population and a tighter
414 range (-5 to -2) for the Late Triassic population (Fig. 5A). The range for the Early Jurassic population
415 overlaps primarily with the Latady Group sedimentary rocks (Fig. 5B) of southern Palmer Land (Fig.
416 1), but not with the coeval Mount Poster Formation (Fig. 1).

417 Two samples from the Late Jurassic Ablation Point Formation (unit 4) have a very different ϵ_{Hf}
418 range than the Atoll Nunataks Formation, which reflects a clear shift in source. Both samples

419 KG.3657.4 and R.2151.30 have ϵHf in the range of +1 to +5, with no clear overlap with known
420 Antarctic Peninsula magmatic events (Fig. 5).

421 Three samples from the Early Cretaceous Himalia Ridge Formation fall in the range -2 to +5, but
422 individual samples have a narrower ϵHf range. The granite clasts from the conglomerate bed (sample
423 KG.3463.2) are in the range of +1 to +2, whilst sample KG.2883.4 is more radiogenic (-2 to +1), and
424 KG.3069.2 is less radiogenic (> +2), despite the relative proximity of the sample sites. The Early
425 Cretaceous population overlaps to some degree with the field for Early Cretaceous granitoids from
426 western Palmer Land (Bastias et al., 2023). This field is likely to trend to more radiogenic values
427 based on the ϵHf values of the granitoid clasts (sample KG.3463.2). Both samples KG.2883.4 and
428 KG.3069.2 have a significant Early Jurassic (ca. 183 Ma) age population with ϵHf values that broadly
429 overlap with those from the Atoll Nunataks Formation (sample KG.3669.24; Fig. 5B).

430 A single sample from the Early Cretaceous Pluto Glacier Formation (sample KG.3969.1) exhibits a
431 relatively tight cluster of ϵHf values (-6 to -2), with very few older zircon grains. The mid-Cretaceous
432 ϵHf values overlap with a field of Early to mid-Cretaceous granitoids examined by Bastias et al.
433 (2023).

434 The youngest sample (ca. 105 Ma) investigated from the Fossil Bluff Group is KG.4956.1 from the
435 Neptune Glacier Formation (Triton Peak Member), which shares a range in ϵHf values (+1 to +7)
436 similar to that of the Pluto Glacier Formation. These values are akin to those of the adjacent mid-
437 Cretaceous granitoids and volcanic rocks of northwest Palmer Land (Riley et al., 2020a; Bastias et al.,
438 2023). A second suite of ages at ca. 125 Ma has a narrower range in ϵHf (-4 to -2) and overlaps with
439 the field of granitoids associated with the Lassiter Coast intrusive suite of eastern Palmer Land (Fig.
440 1; Riley et al., 2018).

441 Also shown in Fig. 5 are the Hf isotopic envelopes from West Antarctica (Nelson and Cottle,
442 2018). These are shown from Marie Byrd Land/Transantarctic Mountains and the Antarctic
443 Peninsula/Thurston Island based on available data at the time. Nelson and Cottle (2018) highlighted

444 that Phanerozoic accretionary orogens exhibit a broadly similar pattern in terms of zircon Hf isotopic
445 evolution reflecting contraction and extension, coupled to slab boundary processes. They identified
446 a Pacific margin-wide Cretaceous–Cenozoic isotopic “pull down” that reflects a strong lithospheric
447 signature during contraction, which is strongly evident in the data presented here from the Fossil
448 Bluff Group and also more recent granitoid/volcanic datasets from Palmer Land (e.g. Riley et al.,
449 2020a; Bastias et al., 2023).

450

451 **5. FOSSIL BLUFF GROUP PROVENANCE ANALYSIS**

452 The U-Pb and Lu-Hf datasets from the Fossil Bluff Group of Alexander Island provide us with a
453 framework for examining the provenance and depositional history of a long-lived forearc basin and
454 for tracing shifts in the continental margin arc magmatism of the Antarctic Peninsula and uplift in
455 late Mesozoic. To evaluate the provenance history of the Fossil Bluff Group we will also examine
456 other sedimentary successions from the Antarctic Peninsula to understand sediment recycling and
457 source-to-sink dynamics. We compare U-Pb and Lu-Hf detrital zircon data from sedimentary rocks
458 from across the Antarctic Peninsula (Trinity Peninsula Group; Erewhon-Mount Peterson beds; Latady
459 Group; Botany Bay Group; Mount Hill Formation, and Le May Group; Fig. 1) to the Fossil Bluff Group
460 dataset (this study). We will also consider late Mesozoic magmatism from the Antarctic Peninsula to
461 investigate direct input from the adjacent arc into a forearc setting and to evaluate whether an
462 autochthonous model for the Western Domain is appropriate.

463

464 **5.1 Comparative Sedimentary Successions**

465 **5.1.1 LeMay Group**

466 The LeMay Group is an ~4-km-thick accretionary complex that underlies, or is in faulted contact
467 with, the Fossil Bluff Group (Fig. 2). It is a succession of variably deformed trench-fill turbidites and
468 trench-slope sediments that are associated with mélangé belts of oceanic floor material (Tranter,

469 1988). Riley et al. (2023) conducted a detailed examination of the provenance and depositional
470 history of the LeMay Group and identified four separate groups. The two main groups have a Late
471 Permian depositional age and an accretionary event in the mid-Triassic during an episode of flat-slab
472 subduction. The other two groups (Group 3: Charcot Island, and Group 4: Mount King; Fig. 2) have
473 considerably younger depositional ages and are not associated with the main accretionary complex.
474 The LeMay Group was interpreted to form part of a series of Late Permian accretionary complexes
475 and volcanoclastic successions along the West Gondwana margin (Riley et al., 2023) from South
476 America to Australia.

477

478 **5.1.2 Trinity Peninsula Group**

479 The Trinity Peninsula Group forms part of the same suite of Late Permian – Triassic accretionary
480 complexes that includes the LeMay Group of Alexander Island. The Trinity Peninsula Group is the
481 dominant geological unit of the northern Antarctic Peninsula and is a ~5-km thick succession of
482 variably deformed siliciclastic turbidites (Hyden and Tanner, 1981). It was incorporated into an
483 accretionary complex, possibly during the Triassic, and has been correlated with the adjacent Scotia
484 Metamorphic Complex (Trouw et al., 1998). Several authors (e.g. Barbeau et al., 2010; Castillo et al.,
485 2015, 2016) have examined the detrital zircon ages of the Trinity Peninsula Group and suggested a
486 likely Permian depositional age with links to the accretionary complexes of Patagonia.

487

488 **5.1.3 Erewhon Nunatak – Mount Peterson beds**

489 Quartz-rich sandstones from Erewhon Nunatak and Mount Peterson in southern Palmer Land
490 (Fig. 1) are interpreted as Late Permian based on detrital zircon analysis and *Glossopteris* flora (Elliot
491 et al., 2016). The sandstones are distinct from the Permian accretionary complexes of the LeMay and
492 Trinity Peninsula groups (Riley et al., 2023), and Elliot et al. (2016) interpreted them as part of a

493 small allochthonous crustal block that is translated from its original position adjacent to the
494 Ellsworth Mountains.

495

496 **5.1.4 Latady Group**

497 The most extensive sedimentary succession of Palmer Land is the Jurassic Latady Group, which
498 developed in a rifted margin setting and forms a succession several kilometers in thickness. Hunter
499 and Cantrill (2006) divided the Latady Group into five separate formations that reflect deposition in a
500 range of settings from coastal to deep marine. U-Pb and Lu-Hf data from detrital zircons of the
501 Latady Group were discussed by Riley et al. (2023) and highlighted a likely depositional age of ca.
502 183 Ma for the lower part of the succession and a Late Jurassic – Early Cretaceous depositional age
503 for the upper part of the succession. The lower part of the Latady Group has a primary detrital zircon
504 age peak identical to the age of the intraplate Mount Poster Formation rhyodacitic volcanic rocks
505 (Pankhurst et al., 2000; Hunter et al., 2006) and was interpreted to form the primary source into rift-
506 controlled basins. The upper part of the Latady Group overlaps with sections of the Fossil Bluff
507 Group and may share common sources, which will be investigated here.

508

509 **5.1.5 Botany Bay Group**

510 The Botany Bay Group is restricted to northern Graham Land (northern Antarctic Peninsula; Fig.
511 1) and forms a succession of terrestrial mudstones, sandstones and conglomerates. The Botany Bay
512 Group is host to abundant plant fossils, which along with the detrital zircon age population (Hunter
513 et al., 2005), suggest a Middle Jurassic depositional age (Farquharson, 1984).

514

515 **5.1.6 Mount Hill Formation**

516 The Mount Hill Formation of eastern Palmer Land (Fig. 1) was considered to be closely related to
517 the Latady Group of southern Palmer Land (Pankhurst et al., 2000); however, only the lower Mount
518 Hill Formation may be similar in depositional age to the upper part of the Latady Group. Detrital
519 zircon data (Riley et al., 2023) indicate that the upper Mount Hill Formation has a considerably
520 younger depositional age (mid-Cretaceous) and may overlap with parts of the Fossil Bluff Group
521 succession.

522

523 ***5.1.7 Palmer Land Cretaceous magmatism***

524 Throughout the late Mesozoic continental margin arc magmatism was widespread across large
525 parts of the Antarctic Peninsula, particularly in Palmer Land and southern Graham Land, broadly
526 adjacent to the forearc basin of Alexander Island. Late Mesozoic arc magmatism has been recorded
527 from ca. 140 to 90 Ma, and was punctuated by several episodes of enhanced magmatism (Riley et al.,
528 2020a; Bastias et al., 2023). Two primary episodes of arc magmatism developed in the intervals 140
529 – 131 Ma and 126 – 100 Ma (Bastias et al., 2023), with a clear hiatus during the Late Jurassic – Early
530 Cretaceous (148 – 140 Ma). More distal to the forearc setting is the Lassiter Coast intrusive suite of
531 eastern Palmer Land which preserves several pulses of granitoid magmatism through the mid-
532 Cretaceous (130 – 102 Ma; Riley et al., 2018; Burton-Johnson et al., 2022).

533

534 **5.2 Fossil Bluff Group: Interpretation**

535 The Fossil Bluff Group of eastern Alexander Island records the exceptional preservation of >8 km
536 of essentially late Mesozoic sedimentary rocks deposited into an accretionary forearc basin that
537 developed adjacent to a late Paleozoic accretionary complex and in proximity to a continental
538 margin arc during a phase of enhanced magmatism. During the late Mesozoic, the Antarctic
539 Peninsula convergent margin was characterised by episodes of magmatic flare-ups that developed
540 during tectonic compression, crustal thickening, and uplift (Burton-Johnson et al., 2022).

541 We used our U-Pb and Lu-Hf detrital zircon data to determine the provenance of the forearc
542 succession and as a monitor for arc magmatic tempos during the late Mesozoic. We used
543 multidimensional scaling (MDS) analysis to evaluate potential correlative units from the Antarctic
544 Peninsula and elsewhere along the West Gondwanan margin.

545 The lowermost Selene Nunatak Formation crops out adjacent to the LeMay Group accretionary
546 complex of central Alexander Island and forms a narrow band of ~150 m in thickness (Fig. 3). The
547 Selene Nunatak Formation has an age profile that is akin to that of the adjacent LeMay Group 1
548 (Riley et al., 2023), with a prominent Late Permian peak and broad spread of Paleozoic ages. The
549 close correlation between the LeMay Group 1 and Selene Nunatak Formation (unit 2) is evident in
550 Figure 6, with both Selene Nunatak Formation samples plotting with a nearest neighbour
551 relationship to LeMay Group 1, which indicates a likely source overlap. There is also a close
552 clustering with samples from the Mount Peterson–Erewhon Beds of the southern Antarctic
553 Peninsula and the Trinity Peninsula Group accretionary complex of the northern Antarctic Peninsula.
554 The close clustering between the LeMay Group and the Mount Peterson-Erewhon Beds was
555 investigated by Riley et al. (2023), who determined that although there is an overlap in age profiles,
556 the Lu-Hf isotopic values are distinct, which suggests a different provenance. The close clustering
557 with the Trinity Peninsula Group reflect a very similar provenance to the LeMay Group, as both units
558 form part of a chain of Late Permian accretionary complexes.

559 The detrital zircon ages therefore strongly support direct recycling of units of LeMay Group 1
560 adjacent to the outcrop extent of the Selene Nunatak Formation and indicate a paleoflow from west
561 to east. Although the age profiles of LeMay Group 1 and the Selene Nunatak Formation are
562 overwhelmingly similar, a single younger age in the Selene Nunatak Formation younger than 200 Ma
563 indicates a potentially younger age of deposition. Based on a weakly diagnostic belemnite
564 assemblage, an approximate Early – Middle Jurassic age is also suggested by Doubleday et al. (1993),
565 who also determined a sediment source from the arc in the east as well as the adjacent accretionary
566 complex in the west.

567 There is an abrupt change in provenance between the Selene Nunatak Formation and the overlying
568 Atoll Nunataks Formation, with a shift in source to the east (arc). The pebble sandstone from the
569 Atoll Nunataks Formation has a prominent Early Jurassic age peak (ca. 183 Ma; Fig. 4C) that is akin to
570 the Early Jurassic component of the Latady Group of southern Palmer Land. However, there is no
571 close clustering between the Atoll Nunataks Formation (unit 3) and the Latady Group in the MDS
572 plot (Fig. 6), which reflects the absence of a broad spectrum of older ages in the Atoll Nunataks
573 Formation. However, the Lu-Hf isotopic data demonstrate a closer relationship (Fig. 5), where an
574 overlap in ϵ_{Hf} values between the Latady Group and the Atoll Nunataks Formation is evident. A likely
575 maximum depositional age of ca. 177 Ma was determined (Fig. S2), which is somewhat older than the
576 proposed Bajocian age (Butterworth et al., 1988).

577 No older U-Pb ages (post-220 Ma) were identified in the Atoll Nunataks Formation that would be
578 anticipated if it was directly recycling components of the Latady Group, which is characterised by an
579 array of Early Paleozoic and Proterozoic ages (Riley et al., 2023). The volcanic input to the Latady
580 Group was widely considered (e.g. Hunter and Cantrill, 2006) to be derived from the neighbouring
581 and essentially contemporaneous Mount Poster Formation (Pankhurst et al., 2000; Hunter et al.,
582 2006). However, the ϵ_{Hf} range of the Mount Poster Formation (ca. 183 Ma) is considerably more
583 radiogenic (-13 to -8; Fig. 5A) than the Early Jurassic component of the Latady Group (-9 to -2; Fig.
584 5A). The implication is that the Early Jurassic (ca. 183 Ma) components of both the Atoll Nunataks
585 Formation and Latady Group were sourced from an episode of Early Jurassic magmatism other than
586 the intraplate Mount Poster Formation (Riley et al., 2001). Early Jurassic arc magmatism is
587 ubiquitous in the southern Antarctic Peninsula (e.g. Riley et al., 2017a; Velev et al., 2023) and the
588 adjacent Thurston Island crustal block (Riley et al., 2017b). The adjacent Brennecke Formation of
589 eastern Palmer Land (Fig. 1) is characterized by intermediate-silicic volcanic rocks, which are distinct
590 in composition from those of the Mount Poster Formation, which have a pronounced upper crustal
591 component (Riley et al., 2001). The Brennecke Formation is less radiogenic and overlaps with the
592 Early Jurassic volcanic rocks of Patagonia and Thurston Island (Riley et al., 2001, 2017b), although no

593 Lu-Hf data are available. Given the absence of a broad spectrum of ages in the age profile of the
594 Atoll Nunataks Formation (Fig. 4C), a proximal Early Jurassic volcanic source is favoured, which is
595 likely to be centered in western Palmer Land or potentially Thurston Island.

596 Interestingly, the Group 3 succession of the LeMay Group (Riley et al., 2023), which has a mid-
597 Cretaceous depositional age (Charcot Island; Fig. 2), is also characterised by a prominent Early
598 Jurassic age population with an ϵ_{Hf} range of -12 to -7 (Fig. 5C), which overlaps with the age of the
599 Mount Poster Formation.

600 The data indicate a significant hiatus (> 20 m.y.) prior to the deposition of the Ablation Point
601 Formation, which forms a ~400-m-thick unit restricted to the eastern margin of Alexander Island and
602 the western coast of northwest Palmer Land (Fig. 3). It has a likely maximum depositional age of ca.
603 155 Ma (Fig. S2), which is consistent with its Kimmeridgian molluscan fauna. The two samples from
604 the Ablation Point Formation have Late Jurassic dominated age profiles (ca. 157 and ca. 153 Ma),
605 combined with a significant contribution from Middle Triassic zircon grains (Figs. 4D and 4E). An age
606 peak of Late Jurassic ages in the Ablation Point Formation overlaps with age profiles from the upper
607 parts of the Latady Group succession (ca. 152 Ma), with both units having similar depositional ages
608 and may share a sediment source. A potential link to the upper Latady Group is also evident in Figure
609 6, with sample KG.3657.4 (unit 4) of the Ablation Point Formation having a nearest neighbour
610 relationship to the Latady Group. However, with additional ϵ_{Hf} data (Fig. 5A), the close relationship
611 between the Ablation Point Formation and the upper Latady Group is not as robust with the ϵ_{Hf}
612 values (at c. 150 Ma) for the upper Latady Group are typically <0, compared to ϵ_{Hf} values of >2 (Fig.
613 5) for the Ablation Point Formation. These ϵ_{Hf} values are amongst the highest across the Fossil Bluff
614 Group and may have coincided with an episode of slab break-off during flat-slab subduction in the
615 Antarctic Peninsula (Bastias et al., 2023).

616 There are no major magmatic sources for the Late Jurassic zircon population evident in the
617 geological record of the Antarctic Peninsula, although minor volcanic units from Adelaide Island

618 (Riley et al., 2012), Alexander Island (Macdonald et al., 1999), and Thurston Island (Riley et al.,
619 2017b) have ages ranging from 155 to 150 Ma. The Middle Triassic contribution to the age profile for
620 the Ablation Point Formation is likely to be sourced from the adjacent granitoids of northwest
621 Palmer Land where Middle to Late Triassic magmatism and metamorphism (Fig. 1) has been widely
622 recognised (Millar et al., 2002; Riley et al., 2020b; Bastias et al., 2023). The detrital zircon age profile
623 for sample KG.3657.4 (Fig. 4E), from near Belemnite Point, has a mixed age population that indicates
624 some degree of recycling of an eroded sediment source, but also a likely proximal Late Jurassic
625 volcanic source.

626 Prior to deposition of the Himalia Ridge Formation there is evidence for a Late Jurassic – Early
627 Cretaceous episode of magmatic quiescence. A magmatic hiatus between ca. 153 – 145 Ma is, to
628 some extent, borne out in the detrital zircon data presented here (Fig. 7), with only limited evidence
629 of magmatism in this interval. Bastias et al. (2023) also suggested a pause in magmatism during the
630 interval 148–140 Ma, but did not link the hiatus to any pause in subduction; instead they favored a
631 model involving increased obliquity during convergence.

632 The Himalia Ridge Formation is an extensive unit, >2.5 km in thickness, and our data indicate a
633 likely depositional age of ca. 140 Ma (Fig. S2), which is consistent with a Tithonian – Berriasian age
634 based on the molluscan fauna (Crame and Howlett, 1988). The succession was deposited as a series
635 of migrating, conglomerate-filled inner-fan channels, with inner-channel mudstone and sandstone
636 facies (Butterworth et al., 1988). The samples investigated here are from the mid to upper part of
637 the succession. The MDS analysis in Fig. 6 indicates that these two samples (KG.3069.2 and
638 KG.2883.4) have a nearest neighbour relationship to the upper part of the Latady Group (Nordsim
639 Formation; Hunter and Cantrill, 2006) which also has a depositional age of ca. 140 Ma (Berriasian).
640 The conglomerate beds in the upper part of the Himalia Ridge Formation are dominated by granitoid
641 clasts instead of volcanic clasts, which Miller and Macdonald (2004) interpreted to represent
642 unroofing of the magmatic arc to the east. The granitoid-only clasts from the Himalia Ridge
643 Formation conglomerate (sample KG.3463.2) can be interpreted as the likely primary arc component

644 of the Himalia Ridge Formation sandstones. The recycled component of the Himalia Ridge Formation
645 sandstones is likely akin to the upper parts of the Latady Group. However, a direct source-to-sink
646 relationship is not favored given the absence of Early Cambrian zircon grains that are ubiquitous in
647 the Latady Group (Riley et al., 2023).

648 Two samples from the Early Cretaceous Spartan Glacier Formation have detrital zircon age
649 profiles very similar to components of the Himalia Ridge Formation, but with marginally younger
650 likely depositional ages (ca. 134 Ma; Fig. S2). The Spartan Glacier Formation has a dominant Early
651 Cretaceous age peak that was likely to be sourced from the adjacent arc, but also a minor recycled
652 component akin to elements of the upper Latady Group, with characteristic Early Jurassic (ca. 184
653 Ma) and mid-Triassic (ca. 218 Ma) age peaks (Figs. 4I and 4J).

654 The Pluto Glacier Formation forms the most extensive unit of the southern and central Fossil Bluff
655 Group. Three samples from across a broad section of the Pluto Glacier Formation all exhibit very
656 similar detrital zircon age profiles (Figs. 4K and 4M). All exhibit a strong primary magmatic arc
657 signature with little input from recycled sources. The ϵ_{Hf} values (Fig. 5A) of the Pluto Glacier
658 Formation closely overlap with the suite of Early Cretaceous granitoids of Palmer Land (Bastias et al.,
659 2023) and support the direct input of a proximal arc source into the shallowing forearc basin. The
660 uppermost Neptune Glacier Formation is almost 3 km in thickness and two samples from the lower
661 and central part of the succession are examined here. Sample J6.288.2 is from Adelaide Island and
662 forms a northern extension of the forearc succession; it is interpreted to form an equivalent unit to
663 the Deimos Ridge Member (unit 8) of Alexander Island. Sample J6.288.2 has a primary age peak of c.
664 115 Ma (two distinct peaks at ca. 112 and ca. 118 Ma; Fig. 4N) and a second Early Cretaceous peak at
665 ca. 134 Ma. Sample KG.4956.1 from the Triton Point Member (unit 9), has a marginally younger age
666 profile, which is characterised by two mid-Cretaceous age peaks at ca. 105 Ma and ca. 124 Ma (Fig.
667 4O). Both samples are dominated by locally sourced input from the adjacent arc with almost no
668 recycling of any early Mesozoic or Paleozoic material. However, there is a significant degree of
669 recycling of mid- to Early Cretaceous material involved in the deposition of the upper parts of the

670 Fossil Bluff Group. Hf data are only available from the uppermost sample from Coal Nunatak
671 (KG.4956.1) which overlaps with the adjacent mid-Cretaceous arc magmatism from northwest
672 Palmer Land (Riley et al., 2020a; Bastias et al., 2023) and the extensive, but more distal Lassiter
673 Coast intrusive suite of eastern Palmer Land (Riley et al., 2018). Samples from the Neptune Glacier
674 Formation have no nearest neighbour relationship or clustering in MDS analysis with any of the pre-
675 Cretaceous sedimentary succession, which indicates that their age profiles are dominated by a
676 proximal arc magmatic input.

677

678 **6. DISCUSSION**

679 The late Mesozoic is one of the most dynamic periods of convergent margin magmatism and
680 tectonic activity across the Antarctic Peninsula, and elsewhere in West Antarctica. However, the late
681 Mesozoic magmatic arc record is unlikely to be complete, because the volcanic units have been
682 eroded, and their intrusive counterparts are unevenly distributed. Also, the direct data record is
683 compromised because access to large sections of the Antarctic Peninsula is not possible due to its
684 terrain and ice cover. Therefore, it is not possible to construct an uninterrupted record of the pulses
685 and pauses in arc magmatism. The detrital zircon age and ϵHf record of a long-lived late Mesozoic
686 forearc basin in Alexander Island has the potential to complement the magmatic record and provide
687 a more complete history of magmatism and subduction dynamics in a continental margin arc setting
688 where zircon is frequently a component of the magmatic rocks. The forearc basin of Alexander Island
689 records a largely complete record of sedimentation through the late Mesozoic and is dominated by
690 litho-feldspathic sandstones, mudstones, conglomerate beds and rare volcanic horizons, with
691 paleocurrent evidence indicating a dominant source to the east from the magmatic arc (Butterworth
692 et al., 1988).

693 Schwartz et al. (2021) suggested the primary sedimentary source for a Cordilleran magmatic
694 forearc basin would be derived from the volcanic carapace and erosion of the uplifted granitoid

695 plutonic belt, and Cawood et al. (2012) demonstrated that forearc settings are dominated by
696 sediment sourced from the proximal arc. Condie et al. (2009) and Schwartz et al. (2021) highlighted
697 that igneous age peaks do not always have detrital counterparts and vice versa, which lends support
698 for examining both the magmatic and detrital record to interpret the tempo of the arc (Surpless et
699 al., 2019). Our analysis of the Fossil Bluff Group, combined with existing analysis of the Mesozoic
700 magmatic record now permits a fuller examination of the coupled arc-basin system.

701 More than 1000 new zircon (U-Pb) analyses are presented, along with 560 zircon (Lu-Hf) analyses,
702 from a suite of 15 samples from across the entire Fossil Bluff Group. Combined U-Pb and Lu-Hf
703 analysis in zircon has been used previously (e.g. Nelson and Cottle, 2018) to infer periods of
704 accelerated extension and contraction at convergent margins. The detrital zircon record is
705 dominated by Cretaceous (n=589) grains sourced from the proximal magmatic arc, with a varying
706 supply of primary and recycled Jurassic grains, as well as recycled Triassic and Paleozoic zircon
707 grains, particularly in the lower parts of the Fossil Bluff Group. Significant zircon age peaks have been
708 identified at ca. 105 Ma, 125–131 Ma, 141 Ma, 154 Ma and 183 Ma (Fig. 7), with notable pauses in
709 magmatism between ca. 120–108 Ma, ca. 152–145 Ma and ca. 177 – ca. 160 Ma (Fig. 7). The mid-
710 Cretaceous magmatic events at ca. 105 Ma, 115 Ma and 125 Ma are well recognised from the
711 southern Antarctic Peninsula, particularly eastern Palmer Land (Lassiter Coast intrusive suite; Riley et
712 al., 2018) and to some extent, central Palmer Land (Flowerdew et al., 2005; Riley et al., 2020a;
713 Bastias et al., 2023). The Early Cretaceous events (ca. 130 Ma and 141 Ma; Fig. 7) are the most
714 significant across the Fossil Bluff Group but are not as ubiquitous in the magmatic record of the
715 Antarctic Peninsula, although Bastias et al. (2023) recognised components of Early Cretaceous
716 magmatism across western Palmer Land, and also central Graham Land. The Late Jurassic age peak
717 at ca. 154 Ma is a prominent feature of the Kimmeridgian Ablation Point Formation and is also a
718 major component of the Latady Group sedimentary rocks of southern Palmer Land (Riley et al.,
719 2023). Magmatism at ca. 155 Ma was recognised by Pankhurst et al. (2000) as representing a
720 significant magmatic pulse (V3 event; 157–153 Ma) across southern Patagonia (Chon Aike Province)

721 but was essentially absent in the magmatic record of the Antarctic Peninsula. However, the detrital
722 zircon record of the Latady Group and the Ablation Point Formation indicates that the V3 event of
723 Patagonia, although largely absent in the volcanic-plutonic record is well-preserved in the detrital
724 record of the forearc and retro/back-arc setting (Latady Group).

725 The Early Jurassic age peak at ca. 183 Ma is prominent in the Atoll Nunataks Formation, forming
726 ~90% of the detrital zircon population, but is also widespread as a secondary age population
727 throughout the Fossil Bluff Group. The Atoll Nunataks Formation has an Early Jurassic (ca. 177 Ma)
728 likely maximum depositional age (Fig. S2), and the Early Jurassic age peak is derived from a proximal
729 arc, and not a recycled source, based on its detrital zircon age profile (Fig. 4C). The source for the
730 Early Jurassic age population is distinct to the widespread Mount Poster Formation of southern
731 Palmer Land, which is characterised by strongly radiogenic ϵ_{Hf} values, whereas the ca. 183 Ma
732 population recorded in the Atoll Nunataks Formation and as subsidiary peaks across the lower part
733 of the Fossil Bluff Group succession has much less radiogenic values (Fig. 5A) and overlaps with parts
734 of the Latady Group (Fig. 5B; Riley et al., 2023). The implication is that an Early Jurassic volcanic
735 source, isotopically distinct from the Mount Poster Formation, which is not preserved in the
736 magmatic record, was present during deposition of the Atoll Nunataks Formation and parts of the
737 Latady Group. The Mount Poster Formation is a suite of rhyodacitic ignimbrites that were strongly
738 controlled by upper crustal processes (Riley et al., 2001) and were emplaced in the interval 185–181
739 Ma (Hunter et al., 2006), likely in an intraplate setting. The ϵ_{Hf} values of ca. 183 Ma zircons from
740 across the Fossil Bluff Group (Fig. 5A) and components of the Latady Group (Fig. 5B) indicate a
741 separate phase of volcanism with a more minor upper crustal component, potentially akin to the
742 Early Jurassic arc magmatism of the Antarctic Peninsula (Riley et al., 2017a). This episode may be a
743 marginally later phase of volcanism associated with the Mount Poster Formation, but with shorter
744 residence times in the upper crust. Interestingly, the mid-Cretaceous sedimentary succession at
745 Charcot Island off the coast of western Alexander Island (Fig. 2) also has a significant Early Jurassic
746 detrital zircon component that overlaps closely with the ϵ_{Hf} values (Fig. 5C) of the Mount Poster

747 Formation (Riley et al., 2023) and indicates a shift in source to sink dynamics during the late
748 Mesozoic. This is also evident from a single Early Jurassic detrital zircon from the mid-Cretaceous
749 Pluto Glacier Formation, which has an ϵ_{Hf} value (~ -8 ; Fig. 5A) that also overlaps with the Mount
750 Poster Formation.

751 The depositional environment for the Atoll Nunataks Formation was considered by Holdsworth
752 and Nell (1992) as a trench-slope setting, as opposed to a forearc basin setting. Given the Early
753 Jurassic depositional age of the lowermost units of the Fossil Bluff Group and a likely 20 m.y. hiatus
754 before the deposition of the Ablation Point Formation, it is likely that the depositional environment
755 of the lowermost sequences of the Fossil Bluff Group are distinct to the main forearc succession,
756 which did not develop until the Late Jurassic. The hiatus between ca. 177 Ma and ca. 155 Ma (Fig. 7),
757 prior to the development of the main phase of forearc deposition, reflects the near absence of
758 magmatism in Palmer Land during the Middle Jurassic, with the main locus of magmatism
759 developing across the northern Antarctic Peninsula. The Mapple Formation (and its correlatives) of
760 northern and eastern Graham Land (Fig. 1) were emplaced in the interval 175–163 Ma (Riley and
761 Leat, 1999; Pankhurst et al., 2000; Riley et al., 2010; Riley and Leat, 2021) and formed part of the V2
762 event of the widespread Chon Aike Province (Pankhurst et al., 1998).

763 Evidence of another significant hiatus in Late Jurassic magmatism in the Antarctic Peninsula has
764 been tentatively suggested by several authors (e.g. Leat et al., 1995; Bastias et al., 2021) but was
765 often based on an incomplete geochronological record from isolated outcrops. The detrital zircon
766 record of the Fossil Bluff Group suggests there may be a minor pause in the magmatic record
767 between ca. 153 Ma and 145 Ma. This pause in magmatism is also identified across Graham Land
768 (Bastias et al., 2021) and Patagonia (Pankhurst et al., 2000) and may correlate with changes in slab
769 dynamics (Nelson and Cottle, 2018), as opposed to any pause in subduction (Bastias et al., 2021).
770 However, a significant pause in continental margin arc magmatism is predicted in some models (e.g.
771 Riley et al., 2001) following magmatic “flare up” events. Throughout the Jurassic, the West
772 Gondwanan margin was punctuated by several high flux magmatic events dominated by silicic

773 volcanism and granitoid emplacement (Chon Aike Province; Pankhurst et al., 1998). High levels of
774 silicic-intermediate magmatism over prolonged periods will deplete the most fusible parts of the
775 crust and inevitably lead to a pause in eruptible magmatism (Bryan et al., 2002). Therefore, the
776 hiatus in magmatism following the emplacement of the Chon Aike Province (188 – 153 Ma;
777 Pankhurst et al, 2000) may be a consequence of changes in crustal processes, rather than any slab
778 dynamic processes.

779 The source-to-sink mechanics of the Fossil Bluff Group are strongly controlled by the supply of
780 sediment from local magmatic sources (cf. Cawood et al., 2012). The absence of any significant
781 population of Middle Jurassic zircon grains (175 – 160 Ma) in the Fossil Bluff Group is strongly
782 suggestive of a strong Palmer Land bias as the primary source into the forearc basin (Fig. 8). Middle
783 Jurassic volcanic and plutonic rocks are widespread in northern and eastern Graham Land, and form
784 an extension of the V2 event of the Chon Aike Province (Pankhurst et al., 2000). By contrast, Middle
785 Jurassic magmatism in Palmer Land is essentially absent, and therefore, a strong Palmer Land source
786 bias for the Fossil Bluff Group is supported. Also, the ubiquitous occurrence of Late Triassic and Early
787 Jurassic age populations in the Fossil Bluff Group strongly indicate a Palmer Land source bias as both
788 age populations are rare in the northern sector of the Antarctic Peninsula. Potential sediment
789 sources farther south (e.g. Marie Byrd Land; Fig. 1) are also unlikely; the ϵ_{Hf} isotopic envelope (Fig.
790 5a) for Marie Byrd Land (Nelson and Cottle, 2018) lies significantly outside the range of the Fossil
791 Bluff Group units, particularly for Triassic – Jurassic components.

792 The uppermost succession exposed in the basin was deposited at ca. 103 Ma (Mars Glacier
793 Member; Moncrieff and Kelly, 1993; Fig. 7) and reflects the large-scale shallowing in the forearc
794 basin. Its deposition was coincident with phase 2 of the Palmer Land tectonic event, an episode of
795 dextral transpression (Vaughan et al., 2012). The event is also associated with the development of
796 unconformities in northwest Palmer Land (Leat et al., 2009), and the compressional event marks the
797 transition to an eventual transtensional regime in the Late Cretaceous (Vaughan et al., 2012). If the
798 Mars Glacier Member represents the cessation of deposition into the forearc basin, it may also

799 overlap with the development of oroclinal bending of the Antarctic Peninsula and Patagonia as a
800 consequence of plate vector changes (Poblete et al., 2016). The Fossil Bluff Group forearc basin
801 underwent exhumation at ca. 100 Ma (Storey et al., 1996), and the underlying LeMay Group
802 accretionary complex also exhibits evidence of compressive deformation associated with this event.

803 Several authors have considered an allochthonous origin for Alexander Island (Vaughan and
804 Storey, 2000; Burton-Johnson and Riley, 2015; Bastias et al., 2023), with terrane translation and
805 “docking” with the Eastern Domain (Fig. 1) of the Antarctic Peninsula occurring during the mid-
806 Cretaceous as part of the Palmer Land Event at ca. 103 Ma (Vaughan et al., 2012). This model implies
807 that the deposition of the entire Fossil Bluff Group developed prior to terrane translation and
808 docking. The provenance signal of the Fossil Bluff Group presented here indicates a strong local bias,
809 with direct recycling of arc material from western Palmer Land during the Cretaceous and a
810 ubiquitous Middle Triassic signal that is also consistent with a likely source from northwest Palmer
811 Land. This age profile could be consistent with the Western Domain forming part of a subduction-
812 accretionary complex with the Central Domain (Vaughan and Storey, 2000). However, the episode of
813 magmatism at ca. 155 Ma that is present in the detrital record of parts of the Fossil Bluff Group
814 (Ablation Point Formation) and also, the Latady Group succession of the Eastern Domain indicates a
815 likely proximal relationship between the Western and Eastern domains during the Late Jurassic.
816 Therefore, an autochthonous model for Alexander Island throughout the Jurassic to the mid-
817 Cretaceous is preferred.

818 The depositional environment and the locus of arc magmatism can have a significant influence on
819 the detrital zircon profile of the sedimentary succession, influencing the variable input of primary
820 and recycled material. The lowermost sequence (Selene Nunatak Formation) is almost entirely
821 composed of recycled material from the adjacent Late Permian accretionary complex (to the west),
822 whereas the overlying Atoll Nunataks Formation is sourced from a proximal Early Jurassic magmatic
823 event into a trench-slope environment (to the east). Following a ~20 m.y. hiatus, the renewed onset
824 of sedimentation into the forearc basin at c. 157 – 153 Ma is dominated by a strongly recycled

825 signature, with Middle Triassic and Paleozoic sources forming a significant component of the
826 Ablation Point and Himalia Ridge formations. Following a brief (~10 m.y.) Late Jurassic hiatus in
827 sedimentation, the Spartan Glacier Formation is also characterised by a mixed arc/recycled
828 signature. But during the Early–mid-Cretaceous, the Fossil Bluff Group is dominated by a primary arc
829 signature from a presumed proximal source in western Palmer Land. This latter phase of deposition
830 into the shallowing forearc basin was significant, with ~4 km of sedimentation preserving a relatively
831 complete arc magmatic record.

832

833 **7. CONCLUSIONS**

834 (1) Deposition in a trench slope environment initiated in the Early Jurassic at ca. 180 Ma. The
835 basal unit of the Fossil Bluff Group (Selene Nunatak Formation) is locally derived from the adjacent
836 Late Permian accretionary complex (LeMay Group), with potentially minor input from the magmatic
837 arc.

838

839 (2) The Early Jurassic signature of the lower Fossil Bluff Group (Atoll Nunataks Formation) is
840 directly derived from a proximal Early Jurassic magmatic source. This source is distinct from the
841 widespread Mount Poster Formation of southern Palmer Land and indicates a separate phase of
842 Early Jurassic (possibly arc) magmatism no longer present in the geological record.

843

844 (3) In Palmer Land, there was a likely hiatus in magmatism and deposition of ~20 m.y. during the
845 Middle Jurassic prior to the onset of forearc sedimentation during the Late Jurassic.

846

847 (4) The V3 event of the widespread Chon Aike Province, which has no significant magmatic record
848 in the Antarctic Peninsula, is well preserved in the Late Jurassic sedimentary record of the Fossil Bluff
849 Group and also the upper Latady Group of eastern Palmer Land.

850

851 (5) The main phase of forearc deposition developed during the Late Jurassic–mid Cretaceous,
852 with a ~6-km-thick sequence directly derived from the late Mesozoic magmatic arc into a shallowing
853 forearc basin (Fig. 8). The episode of Early Cretaceous magmatism (ca. 140 Ma), which is dominant in
854 the detrital record of the Fossil Bluff Group is poorly preserved in the magmatic record.

855

856 (6) Forearc basin deposition is strongly controlled by the proximal arc in western Palmer Land and
857 is characterised by a mixed arc/recycled signature during episodes of renewed sedimentation.
858 However, deposition during the Early Jurassic (ca. 180 Ma) and Early Cretaceous (141–131 Ma) are
859 dominated by arc-only sources.

860

861 (7) ϵ_{Hf} (zircon) records potential tectonic shifts from convergence (Early Jurassic) to extension
862 (Late Jurassic – Early Cretaceous), prior to a strong trend to renewed convergence during the mid-
863 Cretaceous. This reflects the trend identified along large sectors of accretionary orogens of the West
864 Gondwanan margin (Nelson and Cottle, 2018). This trend is clearly defined in the detrital zircon
865 record of the Fossil Bluff Group where previously the direct magmatic record was incomplete.

866

867 (8) The zircon (U-Pb and Lu-Hf) data support an autochthonous origin for the Western and
868 Central domains and a common provenance with the Eastern Domain of the Antarctic Peninsula
869 during the Late Jurassic.

870

871 **ACKNOWLEDGEMENTS**

872 This study is part of the British Antarctic Survey Polar Science for Planet Earth programme, which is
873 funded by the Natural Environmental Research Council. This manuscript has benefited from the
874 helpful comments of John Smellie and an anonymous reviewer. Mark Evans prepared samples for
875 zircon separation, and Kerstin Lindén and Heejin Jeon provided support at the NordSIMS facility. This
876 is NordSIMS contribution number 761.

877 The data that support this research are all available as Supplemental Material files linked to this
878 article. Full datasets are also hosted at the British Antarctic Survey's Polar Data Center via the
879 following link (<https://doi.org/10.5285/F4F0C90E-7ED6-46F4-8973-DD4475C5DCDE>).

880

881 REFERENCES CITED

882 Barbeau, D. L., Davis, J. T., Murray, K. E., Valencia, V., Gehrels, G. E., Zahid, K. M., and Gombosi, D. J.,
883 2010. Detrital-zircon geochronology of the metasedimentary rocks of north-western Graham
884 Land. *Antarctic Science*, v. 22, p. 65-78.

885 Bastias, J., Spikings, R., Riley, T., Ulianov, A., Grunow, A., Chiaradia, M., and Hervé, F., 2021, A revised
886 interpretation of the Chon Aike magmatic province: active margin origin and implications for the
887 opening of the Weddell Sea. *Lithos*, v. 386–387, p. 106013.

888 Bastias, Joaquin, Spikings, Richard, Riley, Teal, Chew, David, Grunow, Anne, Ulianov, Alexey,
889 Chiaradia, Massimo and Burton-Johnson, Alex., 2023, Cretaceous magmatism in the Antarctic
890 Peninsula and its tectonic implications. *Journal of the Geological Society*, v. 180. 18 pp.
891 10.1144/jgs2022-067

892 Bryan, S. E., Riley, T. R., Jerram, D. A. Stephens, C. J., and Leat, P. T., 2002, Silicic volcanism: an under-
893 valued component of large igneous provinces/volcanic rifted margins. In: Menzies, M. A., Klemperer, S.
894 L., Ebinger, C. J. and Baker, J. A., eds. *Volcanic Rifted Margins*, Boulder, Colorado, Geological Society of
895 America Special Paper 363, p. 97-118.

896 Bouvier, A., Vervoort, J. D., and Patchett, P. J., 2008, The Lu–Hf and Sm–Nd isotopic composition of
897 CHUR: constraints from unequilibrated chondrites and implications for the bulk composition of
898 terrestrial planets: *Earth and Planetary Science Letters*, v. 273 (1), p. 8-57.

899 Burton-Johnson, A., and Riley, T. R., 2015, Autochthonous vs. accreted terrane development of
900 continental margins: A new in situ tectonic history of the Antarctic Peninsula. *Journal of the*
901 *Geological Society, London*, v. 172, p. 822-835.

902 Burton-Johnson, A., Riley, T. R., Harrison, R. J., MacNiocaill, C., Muraszko, J. R. and Rowley, P. D.,
903 2022, Granitic magnetic fabrics show tectonic deformation control of episodic continental arc
904 magmatism. *Gondwana Research*, v. 112 10.1016/j.gr.2022.09.006

905 Butterworth, P. J., Crame, J. A., Howlett, P. J., and Macdonald, D. I. M., 1988, Lithostratigraphy of
906 Upper Jurassic-Lower Cretaceous strata of eastern Alexander Island. *Cretaceous Research*, v. 9, p.
907 249-264.

908 Butterworth, P. J., 1991, The role of eustasy in the development of a regional shallowing event in a
909 tectonically active basin, Fossil Bluff Group Jurassic–Cretaceous, Alexander Island, Antarctica. In:
910 Macdonald, D. I. M. ed. *Sedimentation, Tectonics and Eustasy; Sea Level Changes at Active*
911 *Margins. Special Publication of the International Association of Sedimentologists* v. 12, p. 307–
912 329.

913 Castillo, P., Lacassie, J. P., Augustsson, C., and Hervé, F., 2015, Petrography and geochemistry of the
914 Carboniferous-Triassic Trinity Peninsula Group, West Antarctica: Implications for provenance and
915 tectonic setting. *Geological Magazine*, v. 152, p. 575-588.

916 Castillo, P., Fanning, C. M., Hervé, F., and Lacassie, J.P., 2016, Characterisation and tracing of
917 Permian magmatism in the south-western segment of the Gondwana margin: U-Pb age, Lu-Hf
918 and O isotopic compositions of detrital zircons from metasedimentary complexes of northern
919 Antarctic Peninsula and western Patagonia. *Gondwana Research*, v. 36, p. 1-13.

920 Cawood, P. A., Hawkesworth, C. J., and Dhuime, B., 2012, Detrital zircon record and tectonic setting:
921 *Geology*, 40, 875–878. <https://doi.org/10.1130/G32945.1>

922 Condie, K. C., Belousova, E., Griffin, W. L., and Sircombe, K. N., 2009, Granitoid events in space and
923 time: Constraints from igneous and detrital zircon age spectra. *Gondwana Research*, v. 15, p.
924 228–242.

925 Crame, J. A., and Howlet, P. J., 1988, Late Jurassic and early Cretaceous biostratigraphy of the Fossil
926 Bluff Formation, Alexander Island. *British Antarctic Survey Bulletin*, v. 78, p. 1-35.

927 Crame, J. A., and Francis, J. E., 2024, Cretaceous stratigraphy of Antarctica and its global significance.
928 Geological Society, London, Special Publications 545. doi:10.1144/SP545-2023-153

929 Dobbs, S. C., Malkowski, M. A., Schwartz, T. M., Sickmann, Z. T., and Graham, S. A., 2022,
930 Depositional controls on detrital zircon provenance: an example from Upper Cretaceous strata,
931 southern Patagonia. *Frontiers in Earth Science*, 10:824930. doi: 10.3389/feart.2022.824930

932 Doubleday, P. A., and Storey, B. C., 1998, Deformation history of a Mesozoic forearc basin sequence
933 on Alexander Island, Antarctic Peninsula. *Journal of South American Earth Sciences*, v. 11, p. 1–
934 21.

935 Doubleday, P. A., Macdonald, D. I. M., and Nell, P. A. R., 1993, Sedimentology and structure of the
936 trench-slope to forearc basin transition in the Mesozoic of Alexander Island, Antarctica,
937 *Geological Magazine*, v. 130, p. 737-754.

938 Edwards, C. W., 1979, New evidence of major faulting on Alexander Island. *British Antarctic Survey*
939 *Bulletin* v. 49, p. 15-20.

940 Elliot, D. H., Fanning, C. M., and Laudon, T. S., 2016, The Gondwana Plate margin in the Weddell Sea
941 sector: Zircon geochronology of Upper Palaeozoic mainly Permian strata from the Ellsworth
942 Mountains and eastern Ellsworth Land, Antarctica. *Gondwana Research*, v. 29, p. 234-247.

943 Farquharson, G. W. 1984, Late Mesozoic, non-marine conglomeratic sequences of northern Antarctic
944 Peninsula (The Botany Bay Group). *British Antarctic Survey Bulletin*, v. 65, p. 1–32.

945 Flowerdew, M. J., Millar, I. L., Vaughan, A. P. M., and Pankhurst, R. J., 2005, Age and tectonic
946 significance of the Lassiter Coast Intrusive Suite, eastern Ellsworth Land, Antarctic Peninsula:
947 *Antarctic Science*, v. 17, p. 443-452. doi: 10.1017/S0954102005002877.

948 Gao, L., Pei, J. L., Zhao, Y., Yang, Z. Y., Riley, T. R., Liu, X. C., Zhang, S. H., and Liu, J. M., 2021, New
949 paleomagnetic constraints on the Cretaceous tectonic framework of the Antarctic Peninsula.
950 *Journal of Geophysical Research: Solid Earth*, v. 126, p. 1-17.

951 Guenther, W. R., Barbeau Jr., D. L., Reiners, P. W., and Thomson, S. N., 2010, Slab window
952 migration and terrane accretion preserved by low-temperature thermochronology of a magmatic

953 arc, northern Antarctic Peninsula, *Geochem. Geophys. Geosyst.*, v. 11, p. Q03001.
954 doi:10.1029/2009GC002765

955 Hunter, M. A., Cantrill, D. J., Flowerdew, M. J. and Millar, I. L., 2005. Mid-Jurassic age for the Botany
956 Bay Group: implications for Weddell Sea Basin creation and southern hemisphere
957 biostratigraphy. *Journal of the Geological Society, London*, v. 162, p. 745-748.

958 Hunter, M. A., and Cantrill, D. J., 2006, A new stratigraphy for the Latady Basin, Antarctic Peninsula:
959 Part 2, Latady Group and basin evolution. *Geological Magazine*, v. 143, p. 797-819.
960 <https://doi:10.1017/S0016756806002603>.

961 Hunter, M. A., Riley, T. R., Cantrill, D. J., Flowerdew, M. J., and Millar, I. L., 2006, A new stratigraphy
962 for the Latady Basin, Antarctic Peninsula: Part 1, Ellsworth Land volcanic group. *Geological*
963 *Magazine*, v. 143, p. 777-796.

964 Hyden G., and Tanner P. W. G. 1981, Late-Palaeozoic–early Mesozoic forearc basin sedimentary
965 rocks at the Pacific margin in Western Antarctica. *Geologische Rundschau*, v. 70, p. 529-541.

966 Holdsworth, B. K., and Nell, P. A. R. 1992. Mesozoic radiolarian faunas from the Antarctic Peninsula:
967 age, tectonic and palaeoceanographic significance. *Journal of the Geological Society, London*, v.
968 149, p. 1003-1020.

969 Jarrard, R. D., 1986, Terrane motion by strike-slip faulting of forearc slivers. *Geology*, v. 14, p. 780-
970 783.

971 Jeon, H., and Whitehouse, M. J., 2015, A critical evaluation of U–Pb calibration schemes used in SIMS
972 zircon geochronology. *Geostandards and Geoanalytical Research*, v. 39, p. 443-452.

973 Jordan, T. A., Neale, R. F., Leat, P. T., Vaughan, A. P. M., Flowerdew, M. J., Riley, T. R., Whitehouse,
974 M. J., and Ferraccioli, F., 2014, Structure and evolution of Cenozoic arc magmatism on the
975 Antarctic Peninsula; a high resolution aeromagnetic perspective: *Geophysical Journal*
976 *International*, v. 198, p. 1758-1774.

977 Larter, R. D., and Barker, P. F., 1991, Effects of ridge crest–trench interaction on Antarctic–Phoenix
978 spreading: forces on a young subducting plate. *Journal of Geophysical Research: Solid Earth*, v.
979 96, p. 19583–19607.

980 Leat, P. T., Scarrow, J. H., and Millar, I. L., 1995, On the Antarctic Peninsula batholith: *Geological*
981 *Magazine*, v. 132, p. 399-412.

982 Leat, P. T., Flowerdew, M. J., Riley, T. R., Whitehouse, M. J., Scarrow, J. H., and Millar, I. L., 2009,
983 Zircon U-Pb dating of Mesozoic volcanic and tectonic events in north-west Palmer Land and
984 south-west Graham Land, Antarctica. *Antarctic Science*, v. 21, p. 633–641. doi:10.1017/
985 S0954102009990320.

986 Macdonald, D. I. M., and Butterworth, P. J., 1986, Slope collapse deposits in a Mesozoic marine
987 forearc basin, Antarctica. *International Sedimentological Congress, 12th*, Canberra, Australia,
988 Abstracts, p. 193-194.

989 Macdonald, D. I. M., Leat, P. T., Doubleday, P. A., and Kelly, S. R. A., 1999, On the origin of forearc
990 basins: new evidence of formation by rifting from the Jurassic of Alexander Island, Antarctica.
991 *Terra Nova*, v. 11, p. 186–193.

992 Matthews, K. J., Seton, M., and Müller, R. D., 2012, A global-scale plate reorganization event at 105-
993 100 Ma: *Earth and Planetary Science Letters*, v. 355, p. 283–298.

994 McCarron, J. J., and Millar, I. L. 1997, The age and stratigraphy of forearc magmatism on Alexander
995 Island, Antarctica. *Geological Magazine*, v. 134 (4), p. 507-522.

996 Millar, I. L., Pankhurst, R. J., and Fanning, C. M., 2002, Basement chronology and the Antarctic
997 Peninsula: recurrent magmatism and anatexis in the Palaeozoic Gondwana Margin. *Journal of the*
998 *Geological Society, London* v. 159, p. 145-158.

999 Miller, S., and Macdonald, D. I. M., 2004, Metamorphic and thermal history of a forearc basin: the
1000 Fossil Bluff Group, Alexander Island, Antarctica. *Journal of Petrology*, v. 45 (7), p. 1453–1465.
1001 <https://doi.org/10.1093/petrology/egh025>

1002 Milan, L.A., Daczko, N.R., and Clarke, G.L., 2017. Cordillera Zealandia: A Mesozoic arc flare-up on the
1003 palaeo-Pacific Gondwana margin: *Nature Scientific Reports*, v. 7, p, 261.

1004 Moncrieff, A. C. M., and Kelly, S. R. A., 1993, Lithostratigraphy of the uppermost Fossil Bluff Group
1005 Early Cretaceous of Alexander Island, Antarctica: history of an Albian regression. *Cretaceous*
1006 *Research*, v. 14, p. 1–15.

1007 Nell, P. A. R., and Storey, B. C., 1991, Strike-slip tectonics within the Antarctic Peninsula forearc. In
1008 *Geological Evolution of Antarctica* eds. Thomson, M. R. A., Crame, J. A., and Thomson, J.W., pp.
1009 443-8. Cambridge: Cambridge University Press.

1010 Nelson, D. A., and Cottle, J. M., 2018, The secular development of accretionary orogens: linking the
1011 Gondwana magmatic arc record of West Antarctica, Australia and South America: *Gondwana*
1012 *Research*, v. 63, p. 15–33. <https://doi.org/10.1016/J.GR.2018.06.002>

1013 Nichols, G. J and Cantrill, D. J., 2002, Tectonic and climatic controls on a Mesozoic forearc basin
1014 succession, Alexander Island, Antarctica. *Geological Magazine*, v. 139, p. 313-330.

1015 Noda, A., 2016, Forearc basins: Types, geometries, and relationships to subduction zone dynamics.
1016 *Geological Society of America Bulletin*, v. 128, p. 879-895. <https://doi: 10.1130/B31345.1>

1017 Pankhurst, R. J., Leat, P. T., Sruoga, P., Rapela, C. W., Marquez, M., Storey, B. C., and Riley, T. R., 1998, The
1018 Chon-Aike silicic igneous province of Patagonia and related rocks in Antarctica: a ailicic LIP. *Journal of*
1019 *Volcanology and Geothermal Research*, v. 81, p. 113-136.

1020 Pankhurst, R.J., Weaver, S.D., Hervé, F., and Larrondo, P., 1999. Mesozoic – Cenozoic Evolution of the
1021 North Patagonian Batholith in Aysén, Southern Chile: *Journal of the Geological Society, London*, v. 156,
1022 p. 673–694, doi: 10.1144/gsjgs.156.4.0673.

1023 Pankhurst, R. J., Riley, T. R., Fanning, C. M., and Kelley, S. P., 2000, Episodic silicic volcanism in
1024 Patagonia and the Antarctic Peninsula: chronology of magmatism associated with break-up of
1025 Gondwana. *Journal of Petrology*, v. 41, p. 605-625.

1026 Poblete, F., Roperch, P., Arriagada, C., Ruffet, G., de Arellano, C. R., Hervé, F., and Poujol, M., 2016,
1027 Late Cretaceous-early Eocene counterclockwise rotation of the Fueguian Andes and evolution of

1028 the Patagonia-Antarctic Peninsula system. *Tectonophysics*, v. 668, p. 15–34.

1029 <https://doi.org/10.1016/j.tecto.2015.11.025>

1030 Riley, T. R., and Leat, P. T., 1999, Large volume silicic volcanism along the proto-Pacific margin of
1031 Gondwana: lithological and stratigraphical investigations from the Antarctic Peninsula. *Geological*
1032 *Magazine*, v. 136, p. 1-16.

1033 Riley, T. R., Leat, P. T., Pankhurst, R. J., and Harris, C., 2001, Origins of large volume silicic volcanism in the
1034 Antarctic Peninsula and Patagonia by crustal melting. *Journal of Petrology*, v. 42, p. 1043-1065.

1035 Riley, T. R., Flowerdew, M. J., Hunter, M. A., and Whitehouse, M. J., 2010, Middle Jurassic rhyolite
1036 volcanism of eastern Graham Land, Antarctic Peninsula: age correlations and stratigraphic
1037 relationships. *Geological Magazine*, v. 147, p. 581-595.

1038 Riley, T.R., Flowerdew, M.J. and Whitehouse, M.J., 2012, Litho- and chronostratigraphy of a fore- to intra-
1039 arc basin: Adelaide Island, Antarctic Peninsula. *Geological Magazine*, v. 149, p. 768-782.

1040 Riley, T.R., Flowerdew, M.J., Pankhurst, R.J., Curtis, M.L., Millar, I.L., Fanning, C.M., and Whitehouse,
1041 M.J., 2017a, Early Jurassic subduction-related magmatism on the Antarctic Peninsula and
1042 potential correlation with the Subcordilleran plutonic belt of Patagonia. *Journal of the Geological*
1043 *Society, London*, v. 174, p. 365-376.

1044 Riley, T. R., Flowerdew, M. J., Pankhurst, R. J., Leat, P. T., Millar, I. L., Fanning, C. M., and
1045 Whitehouse, M. J., 2017b, A revised geochronology of Thurston Island, West Antarctica and
1046 correlations along the proto-Pacific margin of Gondwana. *Antarctic Science*, v. 29, p. 47-60.

1047 Riley, T. R., Burton-Johnson, A., Flowerdew, M. J., and Whitehouse, M. J., 2018, Episodicity within a
1048 mid-Cretaceous magmatic flare-up in West Antarctica: U-Pb ages of the Lassiter Coast intrusive
1049 suite, Antarctic Peninsula and correlations along the Gondwana margin. *Geological Society of*
1050 *America Bulletin*, v. 130, p. 1177-1196. <https://doi.org/10.1130/B31800.1>.

1051 Riley, T. R., Flowerdew, M. J., Burton-Johnson, A., Leat, P. T., Millar, I. L., and Whitehouse, M. J.,
1052 2020a, Cretaceous arc volcanism of Palmer Land, Antarctic Peninsula: zircon U-Pb geochronology,

1053 geochemistry, distribution and field relationships. *Journal of Volcanology and Geothermal*
1054 *Research*, v. 401, p. 106969.

1055 Riley, T. R., Flowerdew, M. J., Millar, I. L., and Whitehouse, M. J., 2020b, Triassic magmatism and
1056 metamorphism in the Antarctic Peninsula: identifying the extent and timing of the Gondwanide
1057 Orogeny. *Journal of South American Earth Sciences*, v. 103,
1058 <https://10.1016/j.jsames.2020.102732>.

1059 Riley, T. R., and Leat, P. T., 2021. Palmer Land and Graham Land volcanic groups (Antarctic
1060 Peninsula): volcanology. In: Smellie, J. L., Panter, K. S., and Geyer, A. (eds) *Volcanism in*
1061 *Antarctica: 200 Million Years of Subduction, Rifting and Continental Break-up*. Geological Society,
1062 London, Memoirs, 55, <https://doi.org/10.1144/M55-2018-36>

1063 Riley, T. R., Millar, I. L., Carter, A., Flowerdew, M. J., Burton-Johnson, A., Bastias, J., Storey, C. D., Castillo,
1064 P., Chew, D., and Whitehouse, M. J., 2023, Evolution of an accretionary complex LeMay Group and
1065 terrane translation in the Antarctic Peninsula. *Tectonics*. 10.1029/2022TC007578
1066 <https://doi.org/10.1016/j.earscirev.2022.104265>

1067 Robertson, A. H. F., Campbell, H. C., Johnston, M., and Mortimer, N., 2019, Introduction to
1068 Palaeozoic–Mesozoic geology of South Island, New Zealand: subduction-related processes
1069 adjacent to SE Gondwana. In A. H. F. Robertson Ed. *Palaeozoic–Mesozoic Geology of South Island,*
1070 *New Zealand: Subduction-related Processes Adjacent to SE Gondwana*. Geological Society,
1071 London, Memoirs, 49, pp. 1-14.

1072 Schwartz, T. M., Surpless, K. D., Colgan, J. P., Johnstone, S. A., and Holm-Denoma, C. S., 2021,
1073 Detrital zircon record of magmatism and sediment dispersal across the North American
1074 Cordilleran arc system 28–48°N. *Earth-Science Reviews*, v. 220, p. 103734.
1075 <https://doi.org/10.1016/j.earscirev.2021.103734>

1076 Siddoway, C.S., Sass, L.C. III, and Esser, R.P., 2005. Kinematic history of the Marie Byrd Land terrane,
1077 West Antarctica: direct evidence from Cretaceous mafic dykes, *in* Vaughan, A.P.M, Leat, P.T., and

1078 Pankhurst, R.J. *eds.*, Terrane Processes at the Margins of Gondwana. Geological Society, London,
1079 Special Publications, v. 246, p. 417-438.

1080 Simões Pereira, P., van de Flierdt, T., Hemming, S.R., Hammond, S. J., Kuhn, G., Brachfeld, S.,
1081 Doherty, C., and Hillenbrand, C. -D., 2018, Geochemical fingerprints of glacially eroded bedrock
1082 from West Antarctica: Detrital thermochronology, radiogenic isotope systematics and trace
1083 element geochemistry in Late Holocene glacial-marine sediments. *Earth-Science Reviews*, v. 182,
1084 p. 204-232. <https://doi.org/10.1016/j.earscirev.2018.04.011>.

1085 Sláma, J., Košler, J., Condon, D. J., Crowley, J. L., Gerdes, A., Hanchar, J. M., Horstwood, M. S. A.,
1086 Morris, G. A., Nasdala, L., Norberg, N., Schaltegger, U., Schoene, B., Tubrett, M. N., and
1087 Whitehouse, M. J., 2008, Plešovice zircon - a new natural reference material for U–Pb and Hf
1088 isotopic microanalysis. *Chemical Geology*, v. 249 (1–2), p. 1–35.

1089 Smellie, J.L., 2021, Antarctic Peninsula - geology and dynamic development. In: Kleinschmidt, G. (Ed.)
1090 *Geology of the Antarctic continent*. Gebrüder Borntraeger Verlagsbuchhandlung, Stuttgart, pp.
1091 18-86.

1092 Smellie, J.L., and Hole, M.J., 2021, Antarctic Peninsula: volcanology. In: J. L. Smellie J.L., et al.. Eds.
1093 *Volcanism in Antarctica: 200 million years of Subduction, Rifting and Continental Break-up*.
1094 *Geology Society London Memoir*, v. 55, p. 305-325.

1095 Söderlund, U., Patchett, P. J., Vervoort, J. D., and Isachsen, C. E., 2004, The ¹⁷⁶Lu decay constant
1096 determined by Lu–Hf and U–Pb isotope systematics of Precambrian mafic intrusions: Earth and
1097 *Planetary Science Letters*, v. 219 (3), p. 311-324.

1098 Stacey, J. S., and Kramers, J. D., 1975, Approximation of terrestrial lead evolution by a two-stage
1099 model. *Earth and Planetary Science Letters*, v. 26, p. 207-221.

1100 Storey, B. C. and Nell, P. A. R., 1988, Role of strike-slip faulting in the tectonic evolution of the
1101 Antarctic Peninsula. *Journal of the Geological Society, London* v. 145, p. 333-337.

- 1102 Storey, B. C., Brown, R. W., Carter, A., Doubleday, P. A., Hurford, A. J., Macdonald, D. I. M., and Nell,
1103 P. A. R., 1996, Fission-track evidence for the thermotectonic evolution of a Mesozoic – Cenozoic
1104 forearc, Antarctica. *Journal of Geological Society, London*, v. 153, p. 65-82.
- 1105 Surpless, K. D., Clemens-Knott, D., Barth, A. P., and Gevedon, M., 2019, A survey of Sierra Nevada
1106 magmatism using Great Valley detrital zircon trace-element geochemistry: View from the forearc.
1107 *Lithosphere*, v. 11, p. 603-619. doi: 10.1130/L1059.1
- 1108 Taylor, B.J., Thomson, M.R.A., and Willey, L.E., 1979. The geology of the Ablation Point-Keystone
1109 Cliffs area, Alexander Island. *British Antarctic Survey Scientific Reports*, 82, 1-65.
- 1110 Tranter, T. H. 1987, The structural history of the LeMay Group of central Alexander Island,
1111 Antarctica. *British Antarctic Survey Bulletin* v. 74, p. 61-80.
- 1112 Tranter, T. H. 1988, The Tectonostratigraphic history of the LeMay Group of central Alexander Island,
1113 Antarctica. Ph.D. Thesis, Council for National Academic Awards, pp. 272.
- 1114 Trouw, R. A. J., Simoes, L. S. A., and Valladares, C. 1998, Metamorphic evolution of a subduction
1115 complex, South Shetland Islands, Antarctica. *Journal of Metamorphic Geology*, v. 16, p. 475–490.
- 1116 Twinn, G., Riley, T. R., Fox, M., and Carter, A., 2022, Thermal history of the southern Antarctic
1117 Peninsula during Cenozoic oblique subduction. *Journal of the Geological Society, London*,
1118 <https://doi.org/10.1144/jgs2022-008>.
- 1119 Vaughan, A. P. M., and Storey, B. C., 2000, The eastern Palmer Land shear zone: a new terrane
1120 accretion model for the Mesozoic development of the Antarctic Peninsula. *Journal of the*
1121 *Geological Society, London*, v. 157, p. 1243–1256.
- 1122 Vaughan, A. P. M., Pankhurst, R. J., Fanning, C. M., 2002, A mid-Cretaceous age for the Palmer Land
1123 event: implications for terrane accretion timing and Gondwana palaeolatitudes. *Journal of the*
1124 *Geological Society, London*, v. 159, p. 113-116.
- 1125 Vaughan, A. P. M., Eagles, G., and Flowerdew, M. J., 2012, Evidence for a two-phase Palmer Land
1126 event from crosscutting structural relationships and emplacement timing of the Lassiter Coast

- 1127 Intrusive Suite, Antarctic Peninsula: Implications for mid-Cretaceous Southern Ocean plate
1128 configuration. *Tectonics*, v. 31, p. 1010.
- 1129 Velev, S., Lazarova, A., Karaoglan, F., Vassilev, O., and Selbesoğlu, M. O., 2023, Early Jurassic and Late
1130 Cretaceous magmatism on Horseshoe Island, Antarctic Peninsula: New U-Pb and microstructural
1131 data. *Geologica Balcanica* v. 52 (3), p. 29–32.
- 1132 Vermeesch, P., 2018, IsoplotR: a free and open toolbox for geochronology. *Geoscience Frontiers*, v.
1133 9, p. 1479-1493. <https://doi.10.1016/j.gsf.2018.04.001>.
- 1134 Whitehouse, M. J., and Kamber, B. S., 2005, Assigning dates to thin gneissic veins in high-grade
1135 metamorphic terranes: A cautionary tale from Akilia, southwest Greenland. *Journal of Petrology*,
1136 v. 46, p. 291-318.

1137 **List of figures**

1138

1139 Fig.1: Geological map of the Antarctic Peninsula (after Burton-Johnson and Riley, 2015). AP–Antarctic
1140 Peninsula; TI–Thurston Island; MBL–Marie Byrd Land; PLSZ–Palmer Land shear zone; WD–Western
1141 domain; CD–Central Domain; ED–Eastern Domain (Vaughan and Storey, 2000). Core sites in the
1142 Amundsen Sea region (see inset) are from Simões Pereira et al. (2018). Maps were generated in
1143 QGIS geographic information system software.

1144

1145 Fig. 2: Geological map of Alexander Island showing the main lithological units. Approximate positions
1146 of the Fossil Bluff Group sample sites are also shown. More precise localities are shown in Figure 3,
1147 and exact positions are shown in Table S1.

1148

1149 Fig. 3: Updated geological map of the Fossil Bluff Group showing detailed sample sites and division
1150 of the major units (from Butterworth et al., 1988; Crame and Howlett, 1988; Doubleday et al., 1993;
1151 Moncrieff and Kelly, 1993; Nichols and Cantrill, 2002).

1152

1153 Fig. 4: Relative probability density plots of U–Pb detrital zircon ages for a range of sandstone-
1154 siltstone-conglomerate lithologies from the Fossil Bluff Group forearc basin. Kernel density estimator
1155 curves are shown as red dashed lines. Full datasets are available in Table S2. Binwidths for all plotted
1156 samples are 20 Ma.

1157

1158 Fig. 5: U–Pb zircon ages ($^{238}\text{U}/^{206}\text{Pb}$) versus initial ϵHf values for zircon grains analysed in this study
1159 (Table S3). (A) Fossil Bluff Group fore arc basin (this study). Comparative units from 1–Riley et al.
1160 (2020a); 2–Bastias et al. (2023); 3–Riley et al. (2023); 4–BAS unpublished data; 5–Nelson and Cottle
1161 (2018). (B) Latady Group, Botany Bay Group, Mount Hill Formation (Riley et al., 2023). (C) LeMay
1162 Group accretionary complex (Riley et al., 2023). Geochemical envelopes for Marie Byrd Land and

1163 Antarctic Peninsula/Thurston Island are from Nelson and Cottle (2018). CHUR—chondritic uniform
1164 reservoir.

1165

1166 Fig. 6: Multidimensional scaling maps (MDSs; Vermeesch, 2018) comparing the age spectra in
1167 dissimilar samples were calculated using the Kolmogorov-Smirnov statistic. MDS plots map the
1168 degree of similarity between each sample, with any two points plotting closer if they are more
1169 similar. Axis scales are dimensionless and have no physical meaning. MDS plot in this figure shows
1170 ages younger than 600 Ma from the Fossil Bluff Group (this study). Age populations older than 600
1171 Ma are essentially absent (see Fig. 4), and hence were excluded. Sample locations are shown in
1172 Figure 3, where the unit numbers are defined in the stratigraphy. U-Pb zircon data used for MDS
1173 analysis are presented in Table S2. All comparative data are from Riley et al. (2023), and the
1174 locations of lithological units are shown in Figure 1.

1175

1176 Fig. 7: Probability density plot showing the distribution of all Jurassic – Cretaceous ages from the
1177 Fossil Bluff Group and the calculated rates for convergence of the Aluk (Phoenix) Plate with the
1178 Antarctic Peninsula (Riley et al., 2020a). Magmatic and tectonic events are from Pankhurst et al.
1179 (2000), Riley et al. (2018, 2020a), and Bastias et al. (2023).

1180

1181 Fig. 8: Kinematic GPlates reconstruction for the (A) Middle Jurassic and (B) mid-Cretaceous. Adapted
1182 from Riley et al. (2023). Yellow arrows depict potential sediment transport.

1183

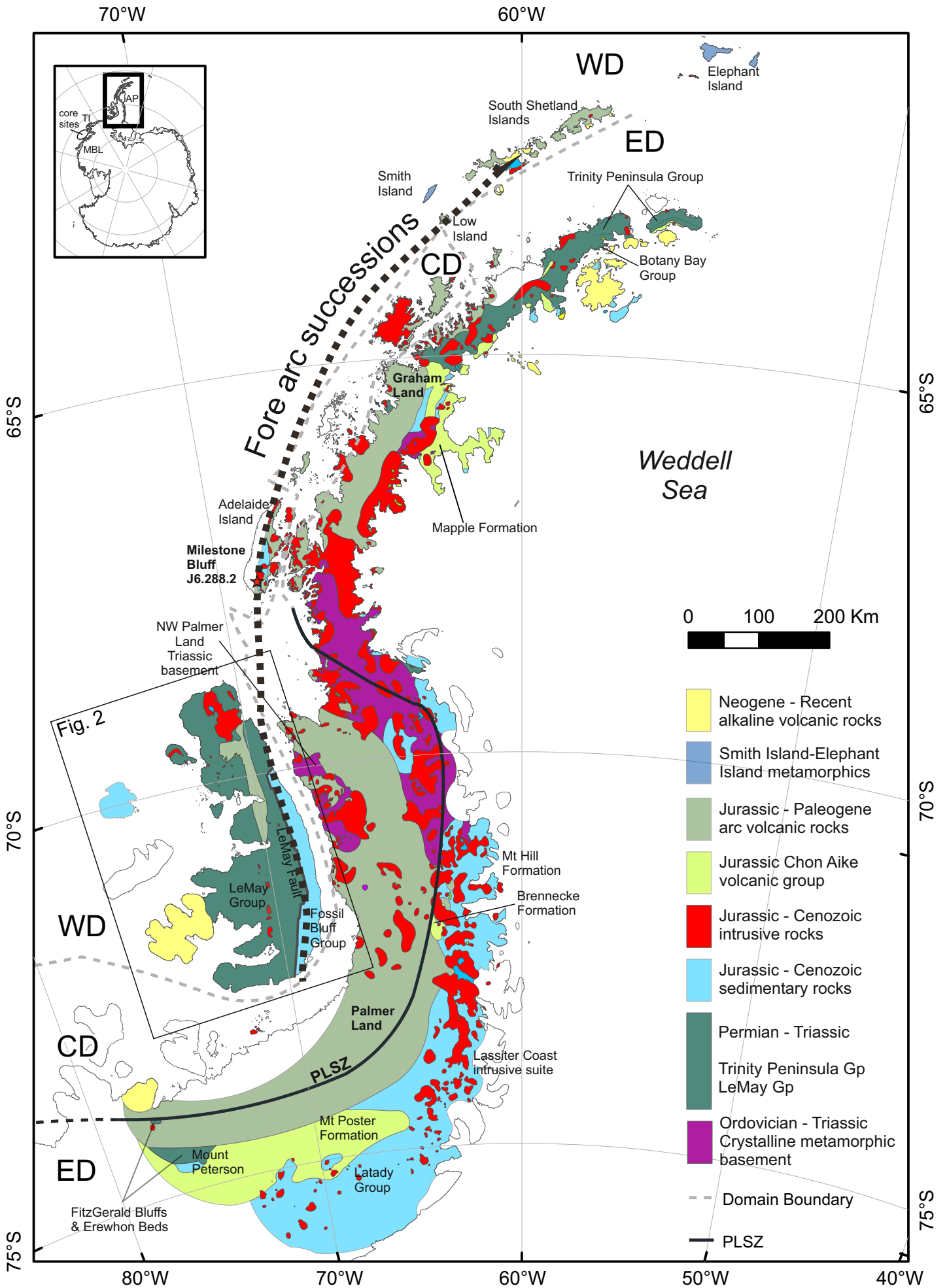


Figure 1

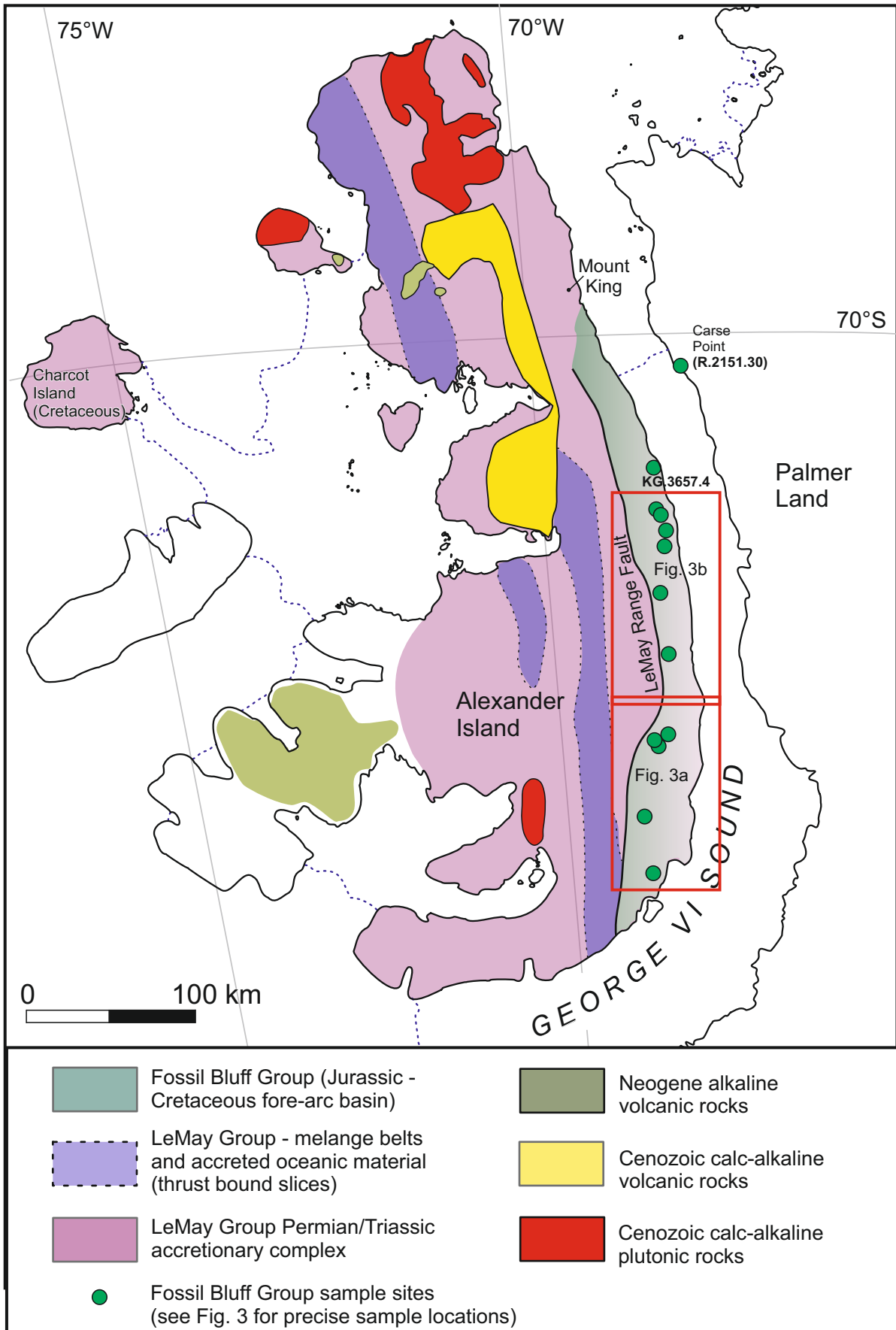


Figure 2

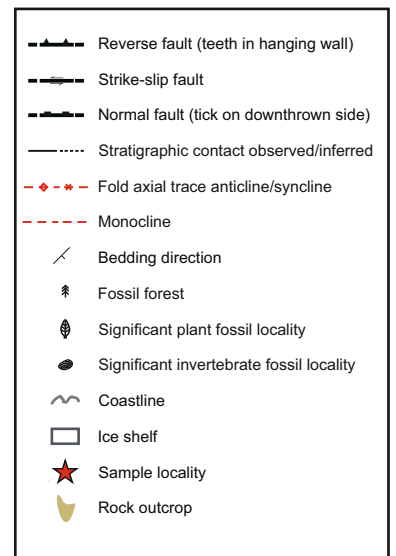
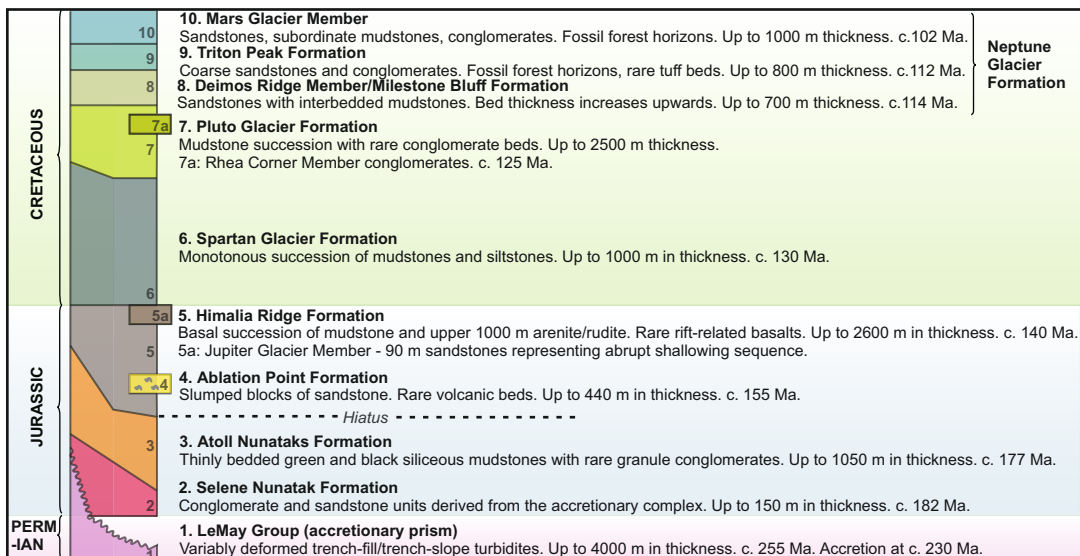
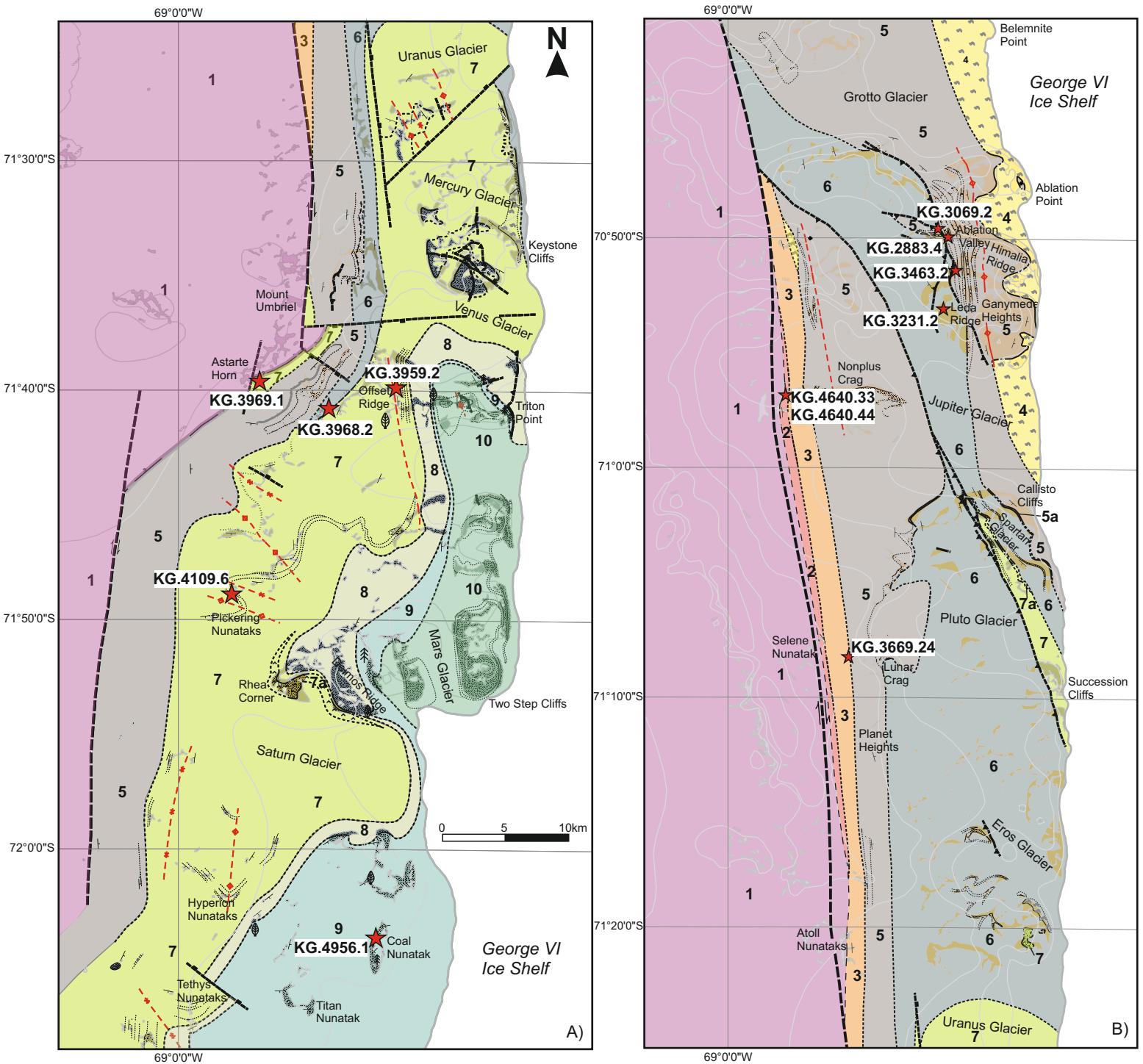


Figure 3

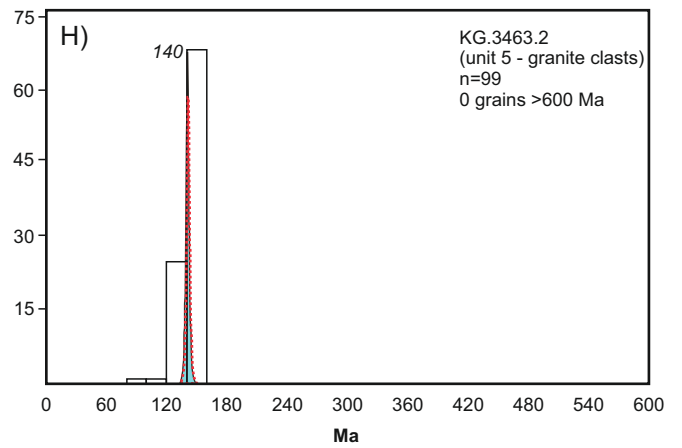
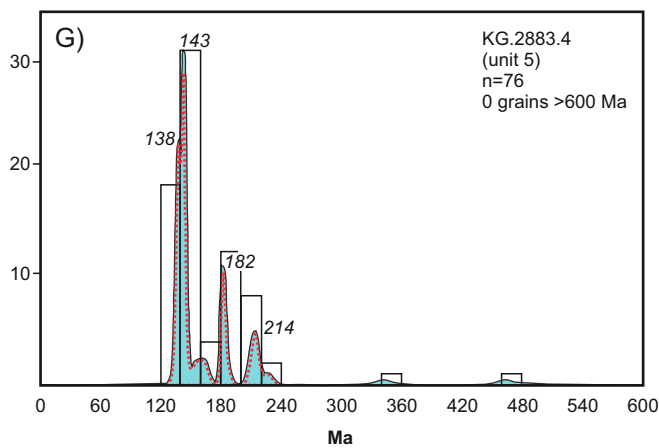
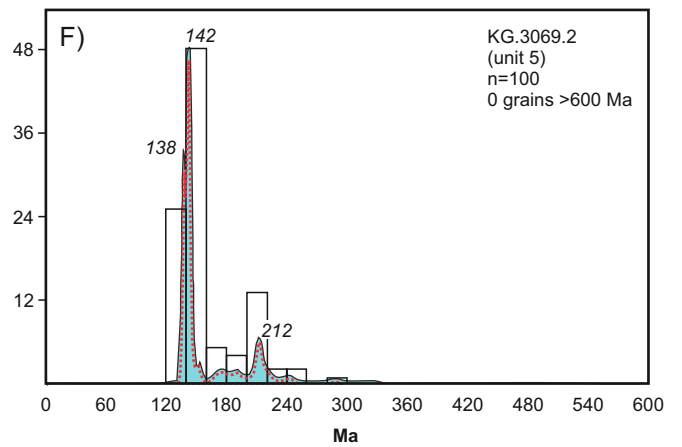
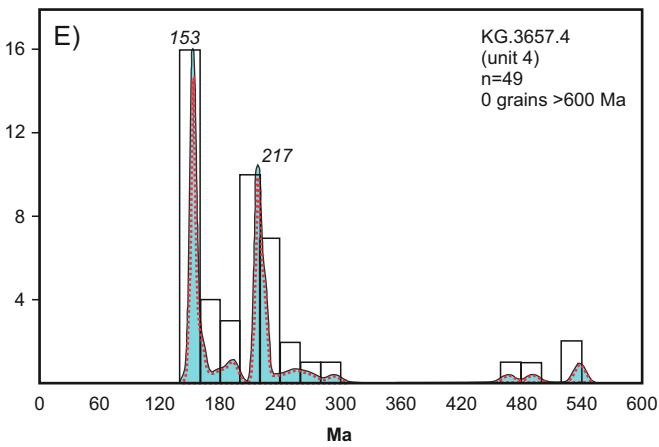
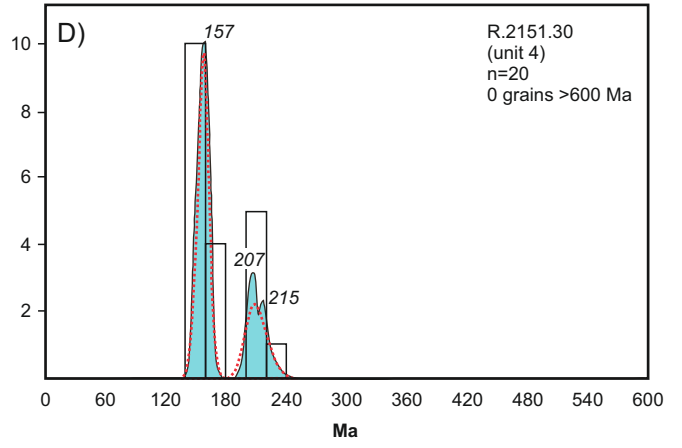
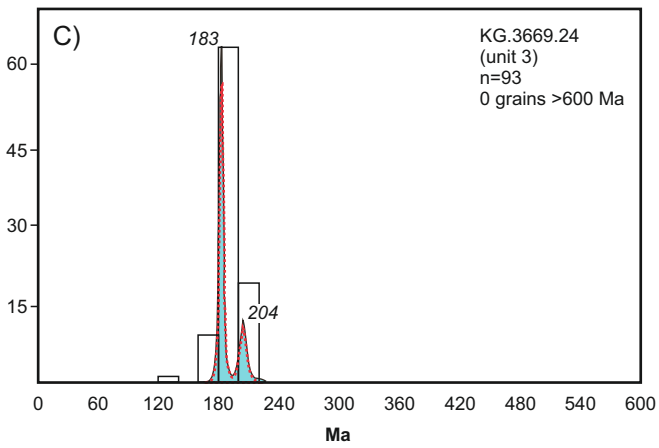
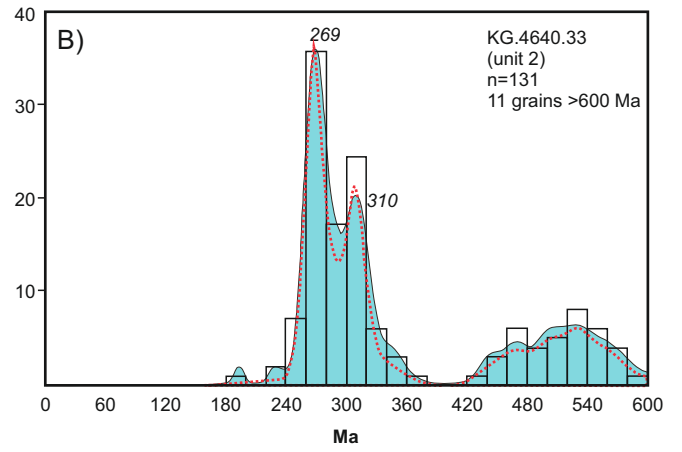
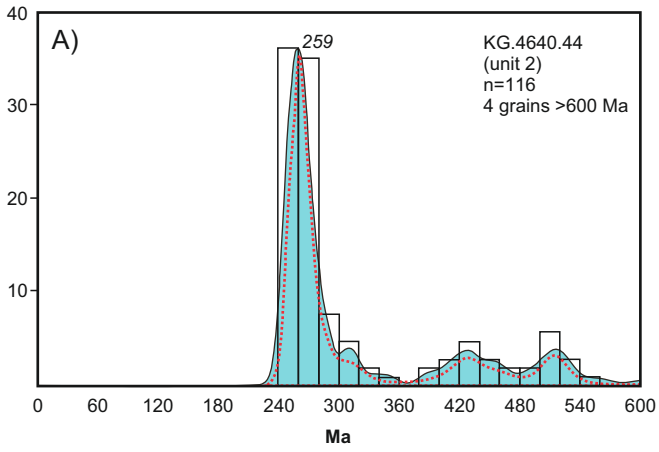


Figure 4

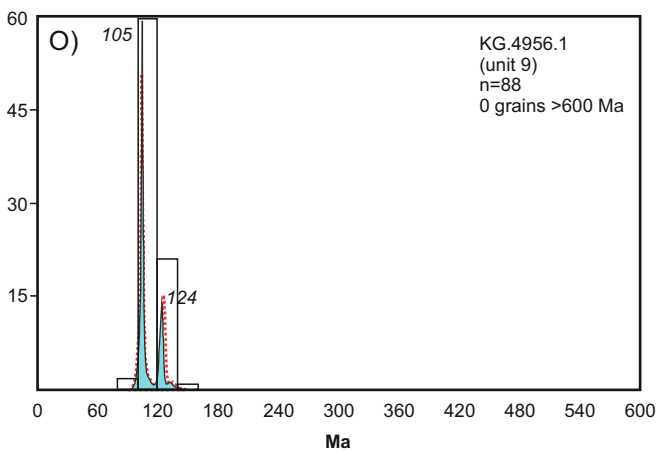
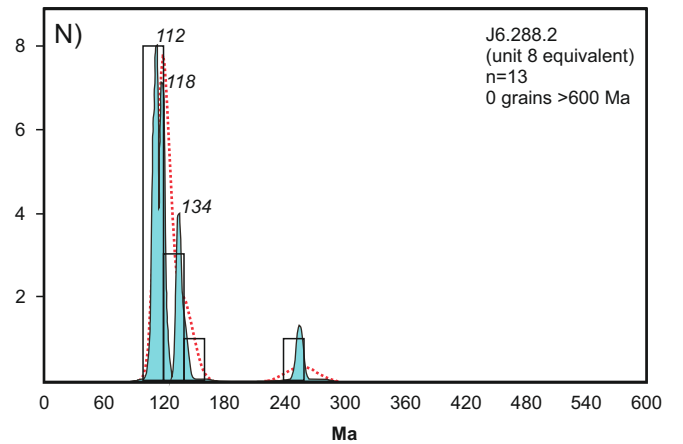
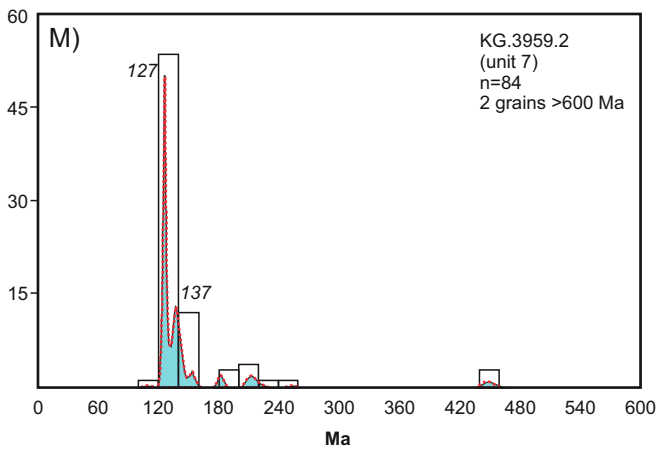
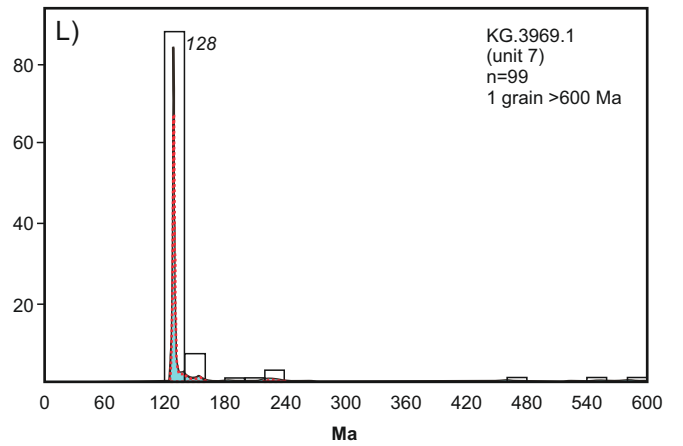
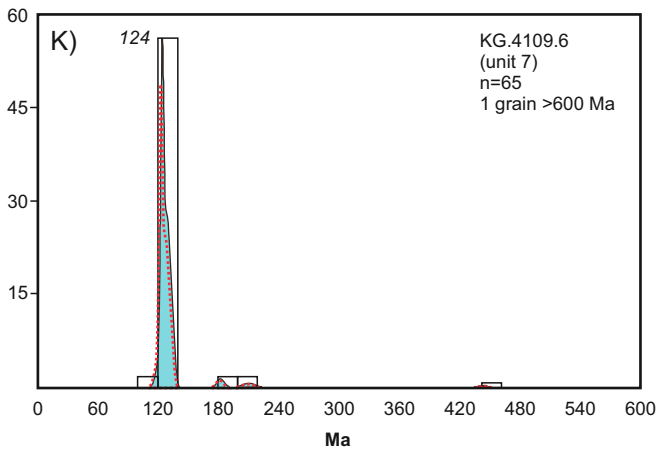
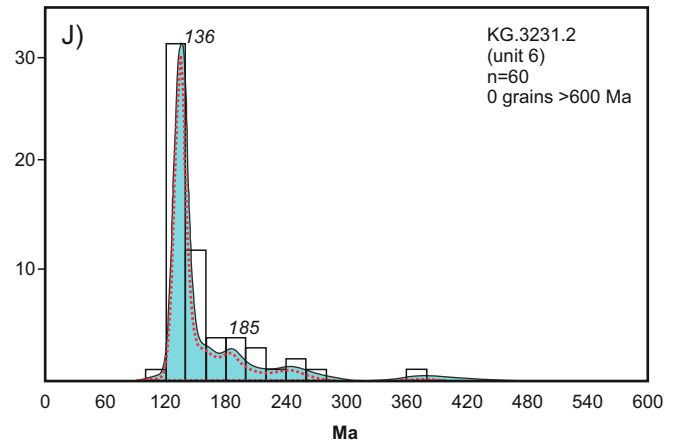
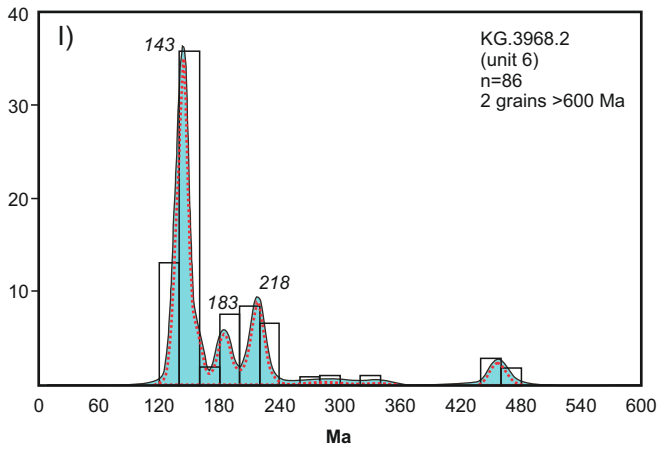


Figure 4



Figure 5

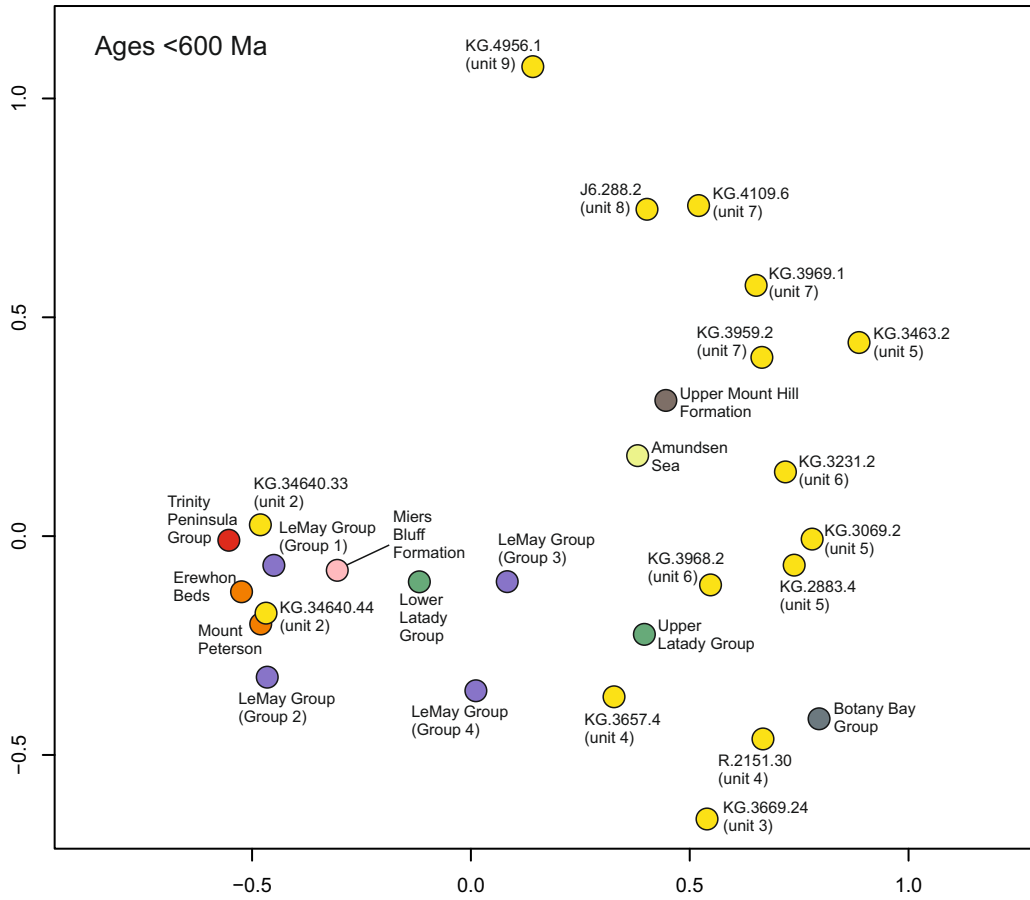


Figure 6

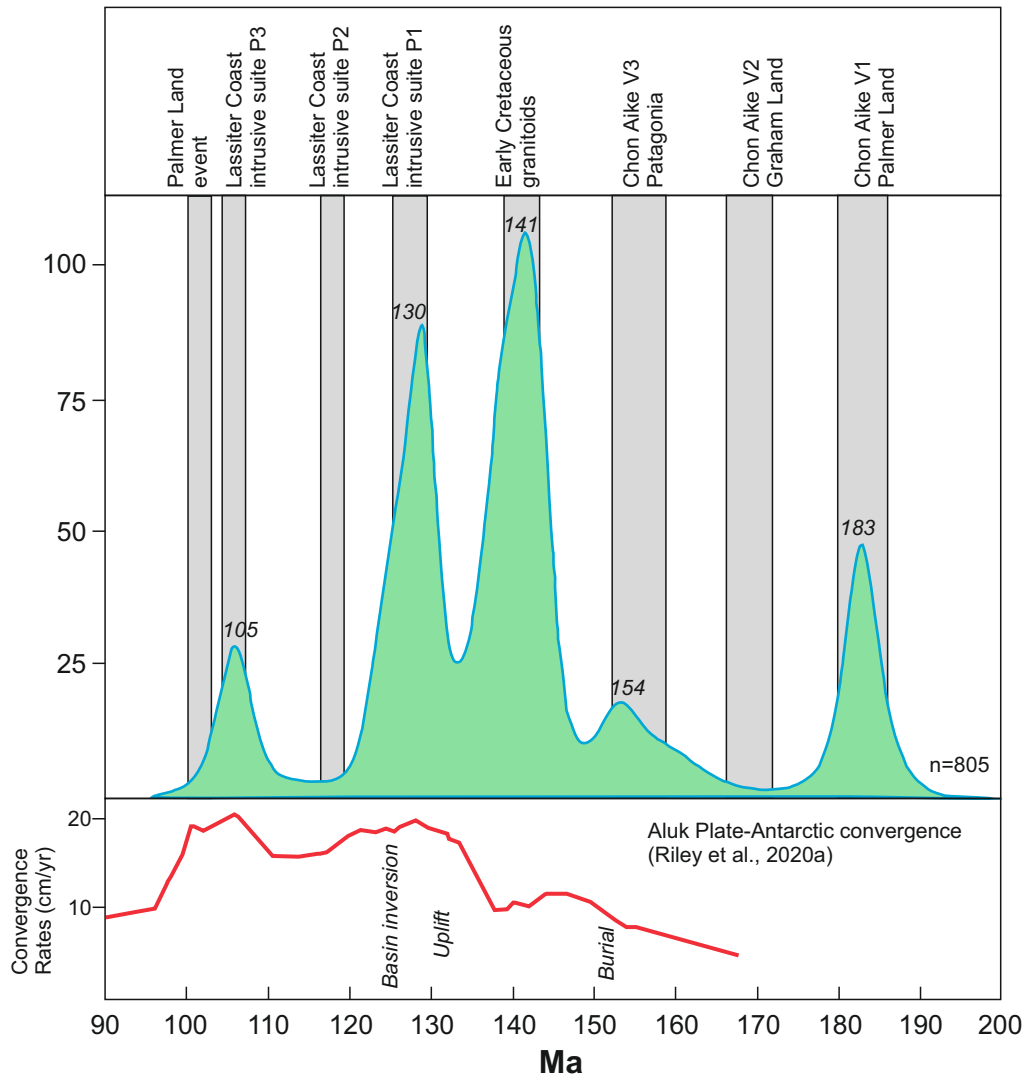


Figure 7

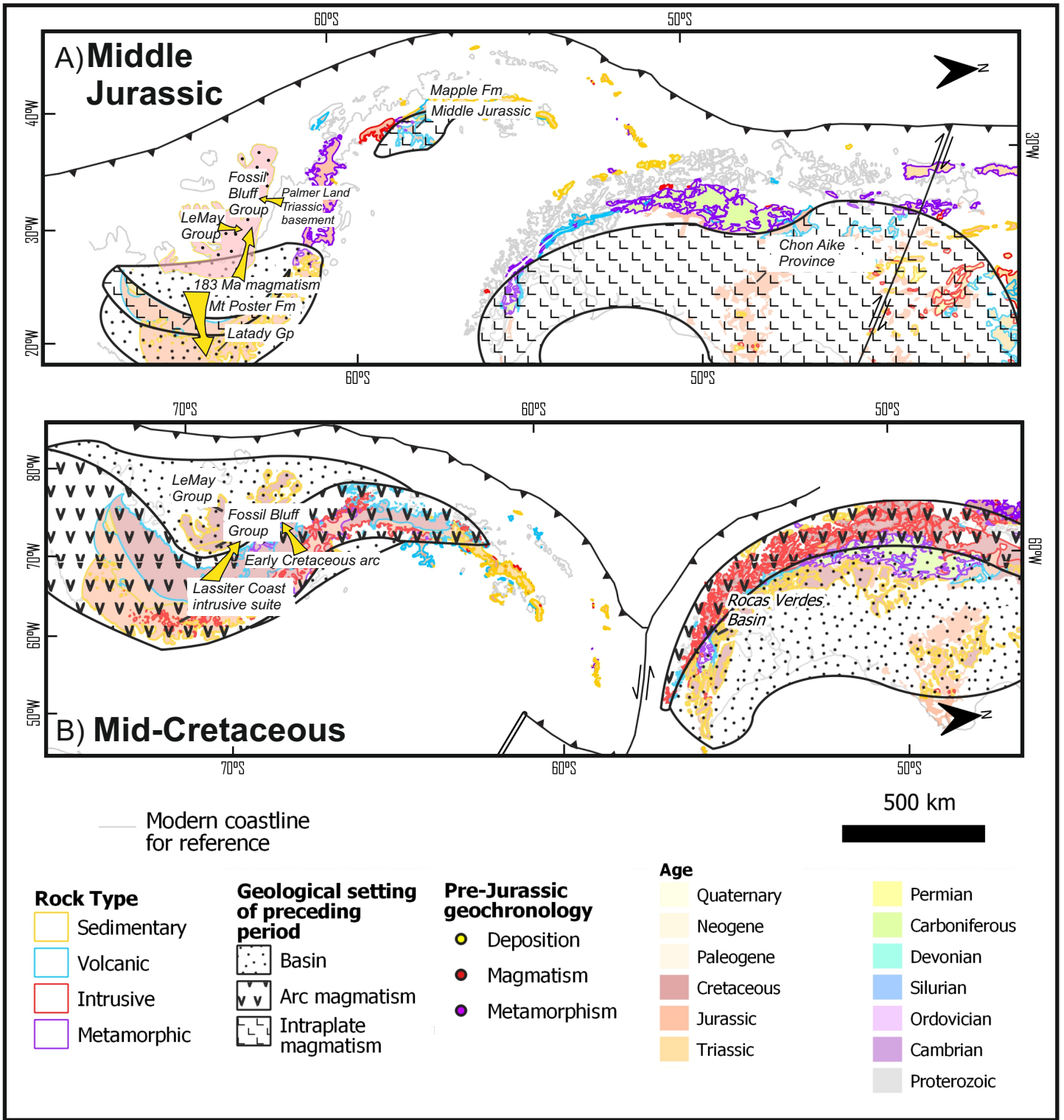


Figure 8